MAGNETIC FLUCTUATION MEASUREMENTS IN THE TOKAPOLE II TOKAMAK

by

Michael Arthur LaPointe

A thesis submitted in partial fulfillment of the requirements for the degree of

Doctor of Philosophy

(Physics)

at the

UNIVERSITY OF WISCONSIN–MADISON

(1990)

MAGNETIC FLUCTUATION MEASUREMENTS IN THE TOKAPOLE II TOKAMAK

Michael Arthur LaPointe

Under the supervision of Professor J. Clinton Sprott
at the University of Wisconsin–Madison

ABSTRACT

Magnetic fluctuation measurements have been made in the Tokapole II tokamak in the frequency range 10 kHz $\leq f \leq$ 5 MHz. The fluctuations above 500 kHz varied greatly as the effective edge safety factor, q_a, was varied over the range $0.8 \leq q_a \leq 3.8$. As q_a was varied from 3.8 to 0.8 the high frequency magnetic fluctuation amplitude increased by over three orders of magnitude. The fluctuation amplitude for 0.5 to 2.0 MHz was a factor of 10 lower than the fluctuation amplitude in the range 100 to 400 kHz for q_a of 0.8. When q_a was increased to 3.8 the difference between the differing frequency ranges increased to a factor of 10^3. Comparison of the measured broadband fluctuation amplitudes with those predicted from thermally driven Alfvén and magnetosonic waves shows that the amplitudes are at least 1000 times larger than the theoretical predictions. This indicates that there is some other mechanism driving the higher

frequency magnetic fluctuations. Estimates show that the contribution by the magnetic fluctuations above 500 kHz to the estimated electron energy loss from stochastic fields is negligible. The profiles of the various components of the magnetic fluctuations indicate the possibility that the shear in the magnetic field may stabilize whatever instabilities drive the magnetic fluctuations.

This work was supported by the National Science Foundation and the United States Department of Energy

Approved

Date

Professor J. Clinton Sprott
Department of Physics

Acknowledgements

There are many people who are responsible for the writing of a thesis and eventual awarding of any individual PhD. There is first and foremost the poor soul who doesn't realize what he is getting himself into. There are the advisors, Prof. J. C. Sprott, who in my case has shown immense patience and understanding, and Prof. S.C. Prager and R.N. Dexter who have provided invaluable discussions and insights. There are the fellow graduate students who through asking or answering questions, making timely comments, having creative (sometimes heated) discussions, or just lending a third hand now and then, help to shape one's thoughts and knowledge. In no particular order I would like to thank S. Assadi, Dr. S.V. Painchaud, Dr. D. Kortbawi, Dr. M. Zarnstorff, Dr. A. Kellman, J. Goetz, I. H. Tan, and E. Haines. You have all helped me one way or another.

To my sisters Karen, Katherine, and Kimberly, I sincerely appreciate all the love, support, and understanding you have given me over the years. Finally, the most important people responsible for my persevering through ten years of graduate school are my parents Arthur and Norma LaPointe. I know how much this has meant to you. It was your love and devotion that sustained me through the bleaker periods. I love you both and dedicate this thesis to you. I only hope that one day I will truly earn the love you have always shown me.

Table of Contents

Chapter 1: Introduction

Measurements of the broadband magnetic fluctuations at frequencies between and including the drift wave and ion cyclotron frequencies in a tokamak plasma are described in this thesis. Also presented are the results of correlation measurements parallel to the equilibrium magnetic field. It is hoped that these results will help in the understanding of turbulence and the resultant transport in magnetic confinement devices.

Transport in various magnetic confinement devices has received increased attention in recent years. A better knowledge of the particle and energy transport mechanisms might allow for increased confinement times and much more modest requirements on the scale and cost of a fusion reactor system. In tokamaks,[1] the measured transport of particles and energy is from ten to one hundred times that predicted by neoclassical diffusion theory.[2–4] The large scale (macroscopic) modes in a plasma and their resultant transport can be overcome by proper choice of machine parameters and are not thought to be a limiting factor in the confinement of a fusion plasma. Small scale (microscopic) turbulence in the plasma density, space potential, temperature, and magnetic field is present in all these devices. Much effort has gone into determining how large an effect the small scale turbulence has on the global confinement.

There is a large body of microinstability theories for the small scale turbulence, as well as models from which the transport can be calculated. With a few exceptions, the theories have been unable to model the measured transport. However, measurements of the plasma turbulence is far from complete. The edge regions of tokamaks are the best diagnosed and comprise the only part of the discharge where all of the fluctuating quantities can be measured simultaneously. This is where microinstability theories have been able to model the observed local transport. [5–7]

There is as yet no conclusive evidence as to the mechanisms by which the bulk of the particles and energy are transported from the center to the edge of a plasma. Measurements using non-intrusive diagnostics[8] of the density and space potential fluctuations have not been able to explain the global confinement properties of the plasmas. For the majority of the confinement devices the particle energies prohibit the use of local probes except in the extreme edge so there is little direct information on the magnetic turbulence levels interior to a tokamak. Efforts are underway to try to measure the magnetic fluctuations interior to a hot plasma[9] using a heavy ion beam probe (HIBP),[10,11] but as yet there are no conclusive results.

Because the Tokapole II is a small, relatively cold tokamak, internal probe measurements of the magnetic fluctuations in a variety of discharges can be made. The purpose of this thesis is twofold. First, a survey of the characteristics of the broadband magnetic fluctuations

between the drift wave and ion cyclotron frequencies ($0.5 \leq f \leq 5$ MHz) was performed. The fluctuation levels for this frequency range are shown to be lower than the levels reported by D. Graessle[12] in the range $10 \leq f \leq 500$ kHz. The broadband spectrum is featureless over most of the frequency range. The frequency integrated fluctuation level decreases with increasing edge q in a way similar to the lower frequency results. The second purpose of this thesis is to measure the correlation length of the magnetic fluctuations parallel to the equilibrium magnetic field. The direction of maximum correlation was found to be indistinguishable from the direction of the equilibrium magnetic field. The parallel correlation length found was greater than the estimate $L_0 \sim qR$, where q is the safety factor and R is the major radius of the device, for lower q discharges.

Comparisons with local transport models could not be done due to a lack of the profile information necessary to determine which microinstability model is appropriate. The confinement is estimated only as a global quantity. Estimates of the thermal transport using stochastic magnetic field models are presented.

This thesis is organized as follows. Chapter 2 give a short review of the experimental and theoretical work related to magnetic turbulence, emphasizing its broadband aspects. Chapter 3 gives a general description of the Tokapole II tokamak and the diagnostics used to obtain the results presented in this paper. Chapter 4 presents the

experimental methods and results of the high frequency and the parallel magnetic fluctuation measurements. Chapter 5 gives a summary of the major results as well some possible directions for future work. An appendix is included which contains the description of the analytic techniques used to perform the statistical analysis necessary for the measurement of the turbulence properties.

References

[1]L. Artsimovich, Nucl. Fusion, **12**, 215 (1972)

[2]*Status of Tokamak Research*, J.M. Rawls, ed., U.S. DOE, Washington D.C., DOE/ER–0034 (1979)

[3]J. Hugill, Nucl. Fusion **23**, 331 (1983)

[4]P.C. Liewer, Nucl. Fusion **25**, 543 (1985)

[5]Ch.P. Ritz, Bengtson, R.D., Levinson, S.J., Powers, E.J., Phys. Fluids, **27**, 2956 (1984)

[6]S.J. Zweben, P.C. Liewer, R.W. Gould, J. Nucl. Mater., **111** & **112**, 39, (1982)

[7]S.J.Levinson, J.M. Beall, E.J. Powers, R.D. Bengtson, Nucl. Fusion, **24**, 527 (1984)

[8]I.H. Hutchinson, *Principles of Plasma Diagnostics*, Cambridge University Press, Cambridge, 1987

[9]P.M. Schoch, R.L. Hickok, V.J. Simcic, X.Z. Yang, Bull. Am. Phys. Soc., **34**, 2153 1989

[10]P.M. Schoch,A. Carnevali, K.A. Conner, T.P. Crowley, J.C. Forster, R.L. Hickok, Rev. Sci. Instrum., **59**, 1646 (1988)

[11]G.H. Hallock, A.J. Wooton, R.L. Hickok, Phys. Rev. Lett., **59**, 1301 (1987)

[12]D. Graessle, PhD Thesis, *Magnetic Turbulence in a Tokamak over Range of Safety Factor* $0.6 \leq q_a \leq 5.0$, University of Wisconsin-Madison, (1988); D. Graessle, S.C. Prager, and R.N. Dexter, Phys. Rev. Lett., **62**, 535 (1989)

Chapter 2: Review of Magnetic Turbulence

Transport has been studied in tokamaks and other machines for many years.[1–5] With few exceptions the theoretical efforts have been unable to describe the measured transport in tokamaks. This has led to the term "anomalous" being used for any measured transport which is greater than collisional neo-classical estimates. Because it has been observed in every confinement device, turbulence has been offered as a possible explanation of the anomalous transport. Turbulence has been observed in the magnetic field, density, electric field, temperature, and every other quantity associated with the plasma. Only turbulence and related transport due to magnetic fluctuations will be presented in this review.

2.1 Transport due to magnetic fluctuations

A short derivation presented in the review article by P. C. Liewer[6] shows how the magnetic fluctuations might contribute to the transport. The particle flux is defined as

$$\Gamma_r = nV_r \tag{2-1}$$

where n is the particle density and V_r is the radial velocity of the fluid. Letting both the density and the velocity consist of equilibrium and

fluctuating components, upon averaging over times long compared to largest fluctuation time scale one gets

$$\Gamma_r = \langle n \rangle \langle V_r \rangle + \langle \tilde{n} \tilde{V}_r \rangle \tag{2-2}$$

where $\langle \cdots \rangle$ represents the time average and $\tilde{n}$, $\tilde{V}_r$ are the fluctuating components of the density and fluid velocity.

For a collisional plasma the particle velocity is often taken for the fluid velocity in eqn. 2-2. In the low frequency limit ($\omega \ll \omega_{ci}$, where ω_{ci} is the ion cyclotron frequency) the particle velocity is given by

$$\tilde{v}_r = c\tilde{E}_p/B + v_{||}\tilde{B}_r/B \tag{2-3}$$

where $\tilde{E}_p$ is the fluctuating poloidal electric field, $v_{||}$ is the velocity of the particle along the unperturbed magnetic field, $\tilde{B}_r$ is the radial component of the fluctuating magnetic field and B is the equilibrium magnetic field. Putting this into equation (2-2) gives

$$\Gamma_r^t = \frac{c\langle \tilde{n}\tilde{E}_p \rangle}{B} - \frac{\langle \tilde{j}_{||}\tilde{B}_r \rangle}{eB} \tag{2-4}$$

where the t superscript denotes the turbulent contribution to the transport and

$$\tilde{j}_{||} = \int_{-\infty}^{\infty} d\vec{v}\, v_{||}\tilde{f}_e \tag{2-5}$$

is the fluctuating parallel current. Correlations between fluctuating quantities can thus drive radial transport. (Note that in this derivation it is possible for the net transport to be inward. Other effects may be involved).

The estimation of the thermal transport due to magnetic fluctuations is a harder problem. The basic problem is to determine the effect of the magnetic fluctuations on the radial thermal transport by the electrons. The classical conductive heat flux[7] is given by

$$\vec{q} = -K_{\|}\nabla_{\|}T - K_{\perp}\nabla_{\perp}T \tag{2-6}$$

where $K_{\|}$ and $K_{\perp}$ are respectively the classical conductivities parallel and perpendicular to the magnetic field. Using a fluid approach and assuming an equilibrium and a fluctuating part to the magnetic field, the radial part of eqn. 2-6 due to the fluctuations can be derived as

$$q_r^t = -K_{\|}\left\langle \left|\frac{\tilde{B}_r}{B}\right|^2 \right\rangle - K_{\|}\left\langle \left|\frac{\tilde{B}_r}{B}\right| \frac{d\tilde{T}}{dx} \right\rangle \tag{2-7}$$

where the t denotes the turbulence. Due to the large classical thermal conductivities, a relatively small fluctuation level ($\tilde{B}/B \approx 10^{-4}$) is sufficient to produce a large heat flux from the plasma. This approach was pursued by Kadomtsev and Pogutse[8] who assumed a stochastic field structure and by Haas, Thayagaraja, and Cook,[9] who made no assumptions on field topology.

There is also the possibility of convective radial transport. Given isotropic pressure fluctuations, the total radial heat flux, including both convective and conductive contributions, is given in the fluid limit by[10]

$$Q_r^t = \frac{5c}{2B}\left\langle \tilde{E}_\theta \tilde{p} \right\rangle \tag{2-8}$$

and is dependent on the correlation of the poloidal electric field fluctuations and the pressure fluctuations. This approach was extended by Mannheimer and Cook[11] to include the effects of magnetic fluctuations. Coupling their results with the drift wave results of Callen,[12] they concluded that the transport due to magnetic turbulence can be as large as the contribution from electrostatic turbulence.

Power balance measurements done on many tokamaks have shown that the loss of thermal energy from the electron and ion conduction channel were the dominant energy loss mechanisms. Most of the 'anomalous' electron thermal losses in ISX–B[13] were attributed to turbulence and other effects. This has caused a lot of effort to be placed on modelling particle and thermal losses from turbulence.

2.2 Transport due to stochastic magnetic fields

The magnetic field in the absence of fluctuations will form flux surfaces, and any radial motion of the particle would be caused only by collisions or well known drifts ($E\times B$, ∇B, *etc.*). If fluctuations are introduced, an island structure is formed, and the particle and fluid

motion will develop a radial component due to motion along the now perturbed magnetic field line. As the amplitude increases, the island structures will begin to overlap, and the magnetic field will start to become braided. If the neighboring island structures are close enough, or the amplitude of the fluctuations are large enough, the magnetic field will become stochastic.[14] In this case there are no flux surfaces remaining in the stochastic region, and the magnetic field line wanders randomly.

Several efforts were made to estimate the electron thermal transport due to the braiding or stochasticity of the magnetic field.[15–21] In 1983, Krommes, Oberman, and Kleva[22] reviewed the test particle approach to stochastic estimates of the electron thermal diffusivity. They showed that the differing results were valid in different collisionality subregimes. The electron thermal transport due to stochastic magnetic fields is often considered the largest contribution that the magnetic fluctuations can make to the overall transport.

Most of the methods of determining the transport from magnetic fluctuations mentioned so far assume a fluctuation spectrum pre–exists. They are not self-consistent in that they do not predict the fluctuation levels nor do they allow for the ensuing particle and thermal transport to modify the fluctuation spectrum. To provide a truly consistent description of the turbulence, theories need to determine not only the fluctuation levels, but also the instabilities which drive them. As there are many sources of free energy in a plasma, many different

theories have been put forth. As yet there is no single, consistent theory which describes all of the measured fluctuation properties.

2.3 Microinstability Models

Microinstability theory has been reviewed by Tang,[23] and Liewer.[2] Horton[24] reviewed the various drift wave theories. Any theory must start with some form of free energy which can drive an instability and eventually transport. The primary sources of free energy in a plasma are gradients in the equilibrium quantities (density, temperature, resistivity, etc). Some possible turbulent modes which can tap this free energy include drift waves, shear–Alfvén waves, and microscopic MHD modes. Because of the reviews listed above, only a cursory discussion will be presented here. Further information can be found in the references.

Drift wave turbulence (see review by Horton[24]) is thought to be one of the most important mechanisms in describing the anomalous transport in tokamaks. Although usually treated in an electrostatic approximation, Callen[12] showed that there could be a small magnetic component which could lead to anomalous transport. Using a fluid model, Waltz[25] simulated electromagnetic drift waves numerically and found that the magnetic fluctuations and the density fluctuations were related by $\tilde{B}_\perp / B = (\beta/2) q \tilde{n}/n$. At modest β (where β is the ratio of the kinetic pressure to the magnetic pressure and q is the local safety factor) the magnetic fluctuations will become dominant. Whether this will

cause the magnetic transport to dominate the drift wave turbulence is still not resolved.

MHD instabilities, when derived from a two fluid or a kinetic approach, can have microturbulent (high poloidal mode number, m) analogs. The two fluid and kinetic descriptions allow inclusion of effects due to finite gyroradius, resonant and trapped particles, differing temperature and density gradients, and parallel (to the equilibrium magnetic field) motion. Various microscopic MHD modes have been investigated. The microtearing mode[26] is driven by the expansion free energy and not by the magnetic energy which drives its macroscopic counterpart. Microtearing modes have been derived from the temperature gradient[27-28] and trapped particles[29] and are estimated to be present in many tokamaks.[27] If diamagnetic effects are included the high–m resistive ballooning modes[30–35] can become unstable. Similar to the ideal MHD ballooning mode,the kinetic ballooning modes[30–35] can become unstable when $\beta > {}^{a}/_{q}{}^{2}R$ where a is the minor radius and R is the major radius of the machine.

Resistivity–gradient–driven–turbulence,[36–38] driven by a parallel current and a gradient in the resistivity, is expected to be important in collisional plasmas with large temperature gradients. Although usually derived as an electrostatic mode, Hahm *et al*[38] derived the magnetic fluctuations and found them to be sensitive to gradients in the impurity profile, temperature and magnetic pitch (shear length).

The relevance of the drift–Alfvén and shear–Alfvén modes[39] to anomalous transport is unclear.[40–42] Although the modes have been

shown to be stable in a system with magnetic shear in both the collisionless[43–45] and collisional limits,[46,47] they can be destabilized by trapped-electron effects,[44,48] temperature gradients,[48] and non-uniformities in the diamagnetic drift frequency.[49] The magnetic fluctuations due to thermally excited Alfvén waves have been calculated.[50] This represents an irreducible minimum for the fluctuations.

Chaos theory has the potential for creating a broadband spectrum from as few as three nonlinearly interacting variables and is a candidate to explain the broadband magnetic fluctuations. Although not a microinstability model, it is included here since is has the potential to determine the number of variables required to describe properly the fluctuations.

The method most employed to date is the measurement of the correlation dimension, ν, for various fluctuating quantities in a plasma. The method for calculating ν is given by Grassberger and Procaccia[51] and consists of calculating the correlation integral

$$C(r) = \lim_{N\to\infty} \frac{1}{N^2} \sum_{i\neq j} \theta(r-|X_i - X_i|) \qquad (2\text{-}9)$$

where θ is the Heavyside step function, $X_i(t) = [x(t_i), x(t_i+p), \ldots, x(t_i+(m-1)p)]$ is an m-dimensional array created from a single time series, p is a time delay, and m is the embedding dimension. The correlation dimension is then defined as

$$\nu = \lim_{r \to 0} d \ln C / d \ln r \qquad (2\text{-}10)$$

and is valid when $\nu < m$.

An incomplete survey of a few experimental efforts shows two basic results. First, for signals with one or more dominant modes present, the relevant correlation dimension is low.[52,53] This suggests that the number of variables needed to describe the signals is relatively low. The dimensions range from 2.1 to 4.8 for the cases with dominant modes. The number of dominant modes found by normal spectral analysis was close to the correlation dimension found, although this may be coincidence. For an arbitrary number of periodic modes it can be demonstrated numerically that the correlation dimension is two, exactly.[54]

The second basic result is that for the broadband turbulence, no definitive correlation dimension has been found.[53,55] For the cases where it has been attempted, the correlation dimension has always been close to the embedding dimension. This implies either the dimension of the turbulence is larger than 10 (the largest quoted in the references listed here) or that the turbulence is random (characterized by $\nu = m$ for all m).

2.4 Other Experimental Work

Magnetic fluctuations have been measured in many tokamaks.

Before discussing individual experiments, several consistent features should be mentioned that have come out of the experiments:

1) the broadband magnetic fluctuations have been seen on every machine in which the measurements were done. The broadband fluctuations were independent of any dominant MHD mode which may have been present in the discharge.

2) correlations between the magnetic fluctuations and other fluctuating quantities ($\tilde{n}$, $\tilde{V}_f$, $\tilde{T}$) are very low and in most cases are indistinguishable from independent sources.

3) correlation lengths of the magnetic fluctuations in tokamaks show that $L_{\|} \gg L_{\theta} \approx L_r$

4) The fluctuations in the r–θ plane are nearly isotropic and much larger (factor of 5-100) than the toroidal fluctuations.

Although the above results are generally true in the tokamaks in which have been measured, there are some other interesting results as well as some discrepancies. A summary of other magnetic fluctuation results is presented. For details of the experiments, one is referred to the references.

MACROTOR

Measurements of the broadband magnetic fluctuations in the frequency range 10–100 kHz were made on Macrotor with probes.[56–57] Except for the MHD modes around 10 kHz, the spectra were featureless. The probes were inserted in to r/a ~ 0.6 where it was found that the

spectral shape was insensitive to radius. The amplitude of the fluctuations increased as the probe was moved into the discharge. At r/a = 0.6 a fluctuation level of $\tilde{B}/B \sim 10^{-4}$ was found. The radial and poloidal fluctuation levels were about equal and were much larger than the toroidal fluctuation level. The relation between the correlation lengths satisfied $L_{\|} \gg L_{\theta} \approx L_{r}$, although no numbers were given. Little or no correlation was seen between the magnetic fluctuations and fluctuations in the density or floating potential.

Caltech Research Tokamak

Hedemann[58–59] found the same general features as those on Macrotor. His measurements included fluctuations in the radial, poloidal, and toroidal directions over the frequency range from 10–1000 kHz. The fluctuation level was $\tilde{B}/B \sim 10^{-3}$. They measured the poloidal correlation length to be around one centimeter. Using the collisionless stochastic model of Rechester and Rosenbluth[15] to estimate the electron energy transport, they observed that the magnetic fluctuations were too small by a factor ten to explain the observed confinement.

ISX–B

Magnetic fluctuation measurements were made in the limiter shadow of ISX–B for frequencies up to 250 kHz.[60-63] The broadband fluctuations exhibited similar behavior to that seen on other machines. The poloidal correlation length was measured to be about five centimeters. With the plasma current held constant, the fluctuation

levels increased with increasing neutral beam power and increasing poloidal beta (=plasma pressure/poloidal magnetic pressure). Increases in the magnetic fluctuations have been correlated with decreases in the global electron energy confinement. For the cases where $\beta_\theta > 1$, an electromagnetic resistive MHD ballooning mode theory[33] has been used to explain the anomalous electron thermal transport and the increase in magnetic fluctuations.

PRETEXT

Levinson *et al*[64] measured the magnetic turbulence in the edge (1 cm inside the limiter) with a probe consisting of four radial coils in a square array. The fluctuation level was $\tilde{B}_r/B \sim 10^{-5}$ over the frequency range 5–250 kHz. From the calculation of fixed pair wavenumber spectra, they showed that turbulence propagated in the electron diamagnetic direction for $f < 100$ kHz. For the higher frequencies the turbulence propagated in the ion diamagnetic direction. These results differed from the electrostatic results previously reported.[65]

TEXT

Kim *et al*[66] reported measurements of the magnetic fluctuations in TEXT. Probes with the frequency response up to 500 kHz were used to within 1 cm of the limiter. A strong correlation was found between the magnetic fluctuations just outside the limiter and density fluctuations inside the limiter. No such correlation was seen for density fluctuations outside the limiter. They also reported that two magnetic coils placed

along a field line were correlated and this correlation was independent of the distance along the line. Measured poloidal mode numbers, from radial falloff and from poloidally separated probes, was ~50. Ritz *et al*[67] used these results to conclude that, in the cold SOL, the energy flux due to magnetic fluctuations is too small by two orders of magnitude to account for the measured energy transport.

McCool *et al*[68] applied external magnetic fields to resonate with the equilibrium field in an attempt to modify the transport. In the region affected by the resonance, they reported that the temperature decreased while the central temperature was relatively unaffected. The particle convection changes were on the order of 30%. The enhancement in the thermal diffusivity was between 15 and 35 m^2/s (a factor of three to six) with $b_r/B \sim 8\times10^{-4}$. When the fields were increased to $b_r/B \sim 1.4\times10^{-3}$, the enhancement was ~190 m^2/s.

TCA

Duperrex *et al*[69] measured magnetic fluctuations between 10 and 1000 kHz in the shadow of the limiter. The broadband turbulence was featureless and decayed as f^{-2}. The poloidal and radial fluctuation levels were about equal and both were three times the toroidal fluctuation level. A strong correlation between increasing magnetic fluctuations and both decreasing density and decreasing confinement time were observed.

Hollenstein *et al*[70] reported results from an edge poloidal Mirnov

array and a separate triaxial probe for frequencies below 500 kHz. The correlation between radial and poloidal fluctuations was small. Poloidal coherence lengths of the poloidal fluctuations were on the order of 10 cm even for higher frequencies. A strong coherence was seen for probes separated by any distance along a q=2 contour. Radial amplitude decay and phase measurements both gave $6 \leq m \leq 8$ for the poloidal fluctuations. Density fluctuations measured with Langmuir probes were unrelated to the magnetic fluctuations in both scaling and spectra. Ryter *et al*[71] have shown that the maximum coherence occurs for displacements along magnetic field lines.

TFTR

Magnetic fluctuation measurements were made by Coster *et al*[72] well behind the limiter on TFTR in the frequency range 1 to 30 kHz. Large coherences were observed for the MHD activity between 1 and 20 kHz. No coherence was seen in the range 20 to 30 kHz between the magnetic fluctuations and the soft x–ray data. Dimensional analysis showed that for the MHD modes, where spectral techniques showed modes with m/n = 2/1 and 3/1, the dimension was low, between one and two. For the turbulent fluctuations the dimension was greater than 10.

Tokapole II

Graessle reported measurements of the magnetic fluctuations both internal and external to the Tokapole II tokamak.[73] Fluctuations were reported to be an decreasing function of edge q over the range $0.6 \leq q_a \leq 5$.

The fluctuations decreased by a factor of 50 over this range. Only at the lowest values of edge q was the fluctuation driven transport consistent with the global transport. The radial profiles of the fluctuations tended to match the local J_{sat} profiles well into the discharge. For $f \geq 150$ kHz, L_p is about $1–2L_r$ indicating that the turbulence is isotropic perpendicular to B. A measurement of the parallel correlation length along a q=1 contour in a q < 1 discharge gave a lower bound of 150 cm. Correlations of the magnetic fluctuations with electrostatic fluctuations were very low.

Other Tokamaks

Magnetic fluctuation measurements have been made on several other tokamaks. Edge broadband fluctuations in the frequency range 0.15–2.0 MHz were observed on the T–4 Tokamak at the Kurchatov Institute in the U.S.S.R.[74] No fluctuation level was given, but it was suggested in the paper that the fluctuations were due to Alfvén instabilities in the interior regions. On the FT–2 Tokamak in Leningrad magnetic fluctuations were observed over the frequency range 0.02–8 MHz.[75] They reported that the spectra decayed with frequency as f^{-2}. They also saw narrow ($\Delta f < f$) peaks on the broadband spectrum which were not associated with the low frequency MHD modes. In the limiter shadow, where the measurements were performed, the magnetic fluctuations decreased as the radius increased. Barnes and Strachan[76] reported broadband magnetic fluctuations up to 100 kHz on PLT. Malacarne and Duperrex[77] showed that for fluctuations on JET in the

frequency range up to 20 kHz, the parallel correlation length is much larger than the perpendicular correlation length. The confinement time is shown to decrease with increases in the magnetic fluctuation levels.

2.5 Motivation for the study of magnetic fluctuations on Tokapole II

The best means of measuring the magnetic fluctuations is with multi-turn coils or pickup loops. However, at distances not far from the edge regions in most tokamaks, the heat load and particle bombardment of a material probe will normally cause the destruction of the probe and possibly contamination of the plasma by high Z impurities. Even for the smaller tokamaks which may only achieve central temperatures of $T_e \sim 100$ eV, the survivability of the material probes can pose problems. Thus, the bulk of the experimental results on magnetic turbulence detailed above have been done in the edge regions of the various machines.

The Tokapole II tokamak is one such small tokamak that can achieve central temperatures of $T_e \sim 100$ eV. Due to a choice of materials for the probe sheath and some novel construction techniques which are described in the next chapter, the magnetic fluctuations both external and internal to the plasma could be measured without degradation to the plasma or the probe.

References

[1]J. Hugill, Nucl. Fusion **23**, 331 (1983)

[2]P.C. Liewer, Nucl. Fusion **25**, 543 (1985)

[3]A.J. Wootton, B. Carreras, H. Matsumoto, K. McGuire, R. McKnight, W.A. Peebles, Ch. Ritz, P.W. Terry and S. Zweben, *Fluctuations and Anomalous Transport in Tokamaks*, Report #340, Fusion Research Center, University of Texas at Austin (1989), submitted to Phys. Fluids.

[4]A.J. Wootton, , *Edge Turbulence*,Fusion Research Center, Report #371, University of Texas at Austin (1990)

[5]F.L. Hinton, R.D. Hazeltine, Rev. Mod. Phys., **48**, 239 (1976)

[6]P.C. Liewer, pp. 551–552

[7]S.I. Braginskii, in *Reviews of Plasma Physics*, ed. by M.A. Leontovich, Consultants Bureau, New York, **1** (1965) 205

[8]B.B. Kadomtsev, O.P. Pogutse, in *Plasma Physics and Controlled Nuclear Fusion Research* (Proc. 7th Intl. Conf. Budapest, 1978) Vol. I, IAEA, Vienna (1979) 649

[9]F.A. Haas, A. Thyagaraja, I. Cook, Plasma Phys., **23**, 1027 (1983); A. Thyagaraja, F.A. Haas, I. Cook, Nucl. Fusion, **20**, 611 (1980)

[10]B.B. Kadomtsev, O.P. Pogutse, in *Reviews of Plasma Physics*, ed. by M.L. Leontovich, Consultants Bureau, New York, **5**, (1970) 249

[11]W.M. Mannheimer, I. Cook, Comments Plasma Phys., **5**(1), 9 (1979)

[12]J.D. Callen, Phys. Rev. Lett., **39**(24), 1540 (1977)

[13]D.W. Swain, M. Murakami, S.C. Bates, C.E. Bush, J.L. Dunlap, P.H. Edmonds, D. Hutchinson, P.W. King, E.A. Lazarus, J.F. Lyon, C.H. Ma, J.T. Mihalczo, L.E. Murray, G.H. Nielson, V.K. Vare, M.J. Saltmarsh, S.D. Scott, C.E. Thomas, J.R. Wilgen, R.M. Wieland, Nucl Fusion, **21**, (1981) 1409; A.J. Wooton, S.C. Bates, C.E. Bush, *Experimental Results on Finite-Beta Limits and Transport in the ISX-B Tokamak*, ORNL Rep. TM-850, (Oct. 1983)

[14]W.M. Mannheimer, C. Lashmore–Davies, *MHD Instabilities in Simple Plasma Configuration*, Naval Research Laboratory, Washington, D.C. (1984) 163

[15]A.B. Rechester, M.N. Rosenbluth, Phys. Rev. Lett., **40**, 38 (1978)

[16]T.H. Stix, Nucl. Fusion, **18**, 353 (1978)

[17]H.E. Mynick, J.A. Krommes, Phys. Rev. Lett., **43**, 1506 (1979)

[18]H.E. Mynick, J.A. Krommes, Phys. Fluids, **23**, 1229 (1980)

[19]V.V. Parail, P.N. Yushmanov, JETP Lett., **42**, 343 (1985)

[20]W. Horton, D.-I. Choi, P.N. Yushmanov, V.V. Parail, Plasma Physics and Controlled Fusion, **29**, 901 (1987)

[21]M. Coronado, J. Vitela-Escamilla, Z. Akcasu, Bull. Am. Phys. Soc., **33**, 1905 (1988)

[22]J.A. Krommes, C. Oberman, and R. Kleva, J. Plasma Physics,**30**, pp11-56 (1983)

[23]W.M. Tang, Nucl. Fusion, **18**, 1089 (1978)

[24]W. Horton, in *Basic Plasma Physics II*, ed. by AA. Galeev and R.N. Sudan, North Holland, 383 (1985)

[25]R.E. Waltz, Phys. Fluids, **28**, 577 (1985)

[26]J.F. Drake, N.T. Gladd, C.S. Liu, C.L. Chang, Phys. Rev. Lett., **44**, 994 (1980)

[27]N.T. Gladd, J.F. Drake, C.L. Chang, C.S. Liu, Phys. Fluids, **23**, 1182, (1980)

[28]Y.C. Lee, J.Q. Dong, P.N. Gusdar, C.S. Liu, Phys. Fluids, **30**, 1331 (1987)

[29]L. Chen, P.H. Rutherford, W.M. Tang, Phys. Rev. Lett., **39**, 460 (1977)

[30]K. Tsang, Phys Fluids, **24**, 2017 (1981)

[31]J.W. Van Dam, PhD Thesis, *Kinetic Theory of Ballooning Instabilities*, UCLA (1979)

[32]A.B. Mikhailovsky, Nucl. Fusion, **13**, 259 (1973)

[33]B.A. Carreras, P.H. Diamond, M. Murakami, J.L. Dunlap, J.D. Bell, H.R. Hicks, J.A. Holmes, E.A. Lazarus, V.K. Pare, P. Similon, C.E. Thomas, R.M. Wieland, Phys. Rev. Lett., **50**, 503 (1983)

[34]P.H. Diamond, P.L. Similon, T.C. Hender, B.A. Carreras, Phys Fluids, **28**, 1116 (1985)

[35]H. Biglari, P.H. Diamond, Phys. Fluids, **30**, 3735 (1987)

[36]B.A. Carreras, P.W. Gaffney, H.R. Hicks, Phys. Fluids, **25**, 1231 (1982)

[37]L. Garcia, P.H. Diamond, B.A. Carreras, J.D. Callen, Phys. Fluids, **28**, 2147 (1985)

[38]T.S. Hahm, P.H. Diamond, P.W. Terry, L.Garcia, B.A. Carreras, Phys. Fluids, **30**, 1452 (1987)

[39]A.B. Mikhailovsky, L.I. Rudakov, Sov. Phys. JETP, **17**, 621 (1963)

[40]P.W. Terry, P.H. Diamond, T.S. Hahm, Phys. Rev. Lett., **57**, 1899 (1986)

[41]A.A. Thoul, P.L. Similon, R.N. Sudan, Phys. Rev. Lett., **59**, 1448 (1987)

[42]J.A. Krommes, C.B. Kim, Phys. Fluids, **31**, 869 (1988)

[43]D.W. Ross, S.M. Mahajan, Phys. Rev. Lett., **40**, 324 (1978)

[44]K.T. Tsang, P.J. Catto, J.C. Whitson, J. Smith, Phys. Rev. Lett., **40**, 327 (1978)

[45]T.M. Antonsen, Phys. Rev. Lett., **41**, 33 (1978)

[46]P.J. Catto, M.N. Rosenbluth, K.T. Tsang, Phys. Fluids, **22**,1284 (1979)

[47]J.F. Drake, R.G. Kleva, Phys. Fluids, **24**, 1499 (1981)

[48]H.R. Strauss, R.D. Hazeltine, S.M. Mahajan, D.W. Ross, Phys. Fluids, **22**, 889 (1979)

[49]A.Y. Aydemir, R.D. Hazeltine, J.D. Meiss, M. Kotschenreuther, Phys. Fluids, **30**, 4 (1987)

[50]Y.Z. Agim, PhD Thesis, *Two-Dimensional Magnetohydromagnetic Equilibria with Flow and Studies of Equilibrium Fluctuations*, University of Wisconsin-Madison (1989); Y.Z. Agim, S.C. Prager, Phys. Fluids B, **2**, 1138 (1990)

[51]P.Grassberger, I. Proccaccia, Physica, **9D**, 189 (1983)

[52]W. Arter, D.N. Edwards, Physics Letters, **114A**, 84 (1986)

[53]G. Ströhlein, A. Piel, Phys. Fluids B, **1**, 1168 (1989)

[54]J.C. Sprott, G. Rowlands, private communication

[55]M.L. Sawley, W. Simm, A. Pochelon, Phys. Fluids, **30**, 129 (1987)

[56]S.J. Zweben, R.J. Taylor, Nucl. Fusion, **21**, 193 (1981)

[57]S.J. Zweben, C.R. Menyuk, R.J. Taylor, Phys. Rev. Lett., **42**, 1270 (1979)

[58]M.A. Hedemann, PhD Thesis, *Measurements of Magnetic Fluctuations in the Caltech Research Tokamak*, California Institute of Technology (1981); M.A. Hedemann, R.W. Gould, Bull. Am. Phys. Soc., **25**, 975 (1980)

[59]S.J. Zweben, P.C. Liewer, R.W. Gould, J. Nucl. Mater., **112** & **113**, 39 (1982)

[60]B.A. Carreras, R.C. Isler, J.L. Dunlap, L.E. Murray, J.D. Bell, L.A. Charlton, W.A. Cooper, R.A. Dory, T.C. Hender, H.R. Hicks, J.T. Hogan, J.A. Holmes, H.C. Howe, E.A. Lazarus, D.K. Lee, V.E. Lynch, J. Munro, M. Murakami, A.P. Navarro, G.H. Nielson, V.K. Paré, K.E. Rothe, D.J. Sigmar, R.M. Wieland, A.J. Wooton, P.H. Diamond, P.L. Similon, in *Plamsa Physics and Controlled Nuclear Fusion Research* (Proc. 9th Intl. Conf. Baltimore, 1982) Vol. III, IAEA, Vienna (1983) 77

[61]M. Murakami, S.C. Bates, J.D. Bell, C.E. Bush, A. Carnevali, B.A. Carreras, J.L. Dunlap, P.H. Edmonds, O.C. Eldridge, A.C. England, W.L. Gardner, J.H. Harris, H,C. Howe, D.P. Hutchinson, R.C. Isler, T.C. Jernigan, R.R. Kindsfather, P.W. King, R.A. Langley, E.A. Lazarus, J.F. Lyon, C.H. Ma, P.K. Mioduszewski, L.E. Murray, G.H. Nielson, V.K. Paré, M.J. Saltmarsh, S.D. Scott, D.J. Sigmar, J.E. Simpkins, K.A. Stewert, W.L. Stirling, C.E. Thomas, R.M. Wieland, J.B. Wilgen, W.R. Wing, A.J. Wooton, ibid., Vol. 1, (1983) 57

[62]B.A. Carreras, J.L. Dunlap, W.A. Cooper, *MHD Activity in the ISX–B Tokamak: Experimental Results and Theoretical Interpretation*, Oak Ridge National Laboratory Report TM–8648 (June 1983)

[63]A.J. Wooton, S.C. Bates, C.E. Bush, *Experimental Results of Finite–Beta Limits and Transport in the ISX–B Tokamak*, Oak Ridge National Laboratory Report TM–8750 (Oct 1983)

[64]S.J. Levinson, B. Rogers, E.J. Rogers, R.D. Bengtson, Bull. Am. Phys. Soc., **30**, 1441 (1985)

[65]S.J. Levinson, J.M. Beall, E.J. Powers, R.D. Bengtson, Nucl. Fusion, **24**, 527 (1982)

[66]Y.J. Kim, K.W. Gentle, C.P. Ritz, T.L. Rhodes, R.D. Bengtson, Nucl. Fusion, **29**, 99 (1989)

[67]Ch. P. Ritz, R.V. Bravenec, P.M. Schoch, R.D. Bengtson, J.A. Boedo, J.C. Forster, K.W. Gentle, Y. He, R.L. Hickok, Y.J. Kim, H. Lin, P.E. Phillips, T.L. Rhodes, W.L. Rowan, P.M. Valanju, A.J. Wooton, Phys. Rev. Lett., **62**, 1844 (1989)

[68]S.C. McCool, A.J. Wooton, A.Y. Aydemir, R.D. Bengtson, J.A. Boedo, R.V. Bravenec, D.L. Brower, J.S. DeGrassie, T.E. Evans, S.P. Fan, J.C. Forster, M.S. Foster, K.W. Gentle, Y.X. He, R.L. Hickok, G.L. Jackson, S.K. Kim, M. Kotschenreuther, N.C. Luhmann,Jr., W.H. Miner,Jr., N Ohyabu, D.M. Patterson, W.A. Peebles, P.E. Phillips, T.L. Rhodes, B. Richards, C.P. Ritz, D.W. Ross, W.L. Rowan, P.M. Schoch, B.A. Smith, J.C. Wiley, X.H. Yu, S.B. Zheng, Nucl. Fusion, **29**, 547 (1989)

[69]P.A. Duperrex, Ch. Hollenstein, B. Joye, R. Keller, J.B. Lister, F.B. Marcus, J.M. Moret, A. Pochelon, W. Simm, Physics Letters, **106A**, 133 (1984); P.A. Duperrex, PhD Thesis, *Measurement of Magnetic Fluctuations in the JET and TCA Tokamak,* Ecole Polytechnique Fédérale de Lausanne (1988)

[70]Ch. Hollenstein, R. Keller, A. Pochelon, F. Ryter, M.L. Sawley, W. Simm, H. Weisen, in *Proceedings of the Cargèse Workshop*, 1986, ed. by D. Grésillon and M.A. Dubois, (1986); Lausanne internal

report LRP 306/86

[71]F.Ryter, A. Pochelon, F. Hofmann, in *Proceeding of the 14th European Conference on Controlled Fusion and Plasma Physics, Madrid, 1987*, ed. by S. Methfessel (EPS, Petit-Lancy, 1987)

[72]D.P. Coster, E.D. Fredrickson, K.M. McGuire, A.W. Morris, Bull. Am. Phys. Soc., **33**, 2096 (1988)

[73]D.Graessle, PhD Thesis, *Magnetic Turbulence Versus Safety Factor in the Tokapole II Tokamak*, University of Wisconsin-Madison, (1989); D.Graessle, S.C. Prager, R.N. Dexter, Phys. Rev. Lett., **62**, 535 (1989)

[74]N.V. Ivanov, I.A. Kovan, I.B. Semenov, Sov. J. Plasma Phys., **3**, 526 (1977)

[75]V.V. Bulanin, L.A. Esipov, D.O. Korneev, A.Yu. Stepanov, S.N. Ushakov, N.V. Yashukova, Sov. J. Plasma Phys., **15**, 147 (1989)

[76]C.W. Barnes, J.D. Strachan, Phys. Fluids, **26**, 2668 (1983)

[77]M. Malacarne, P.A. Duperrex, Nucl. Fusion, **27**, 2113 (1987)

Chapter 3: Description of the Apparatus

3.1 The Tokapole II Tokamak

The experimental results presented in this thesis were obtained on the Tokapole II tokamak at the University of Wisconsin-Madison[1]. The Tokapole II tokamak (Figure 3.1) is a small, poloidal divertor tokamak capable of operation over a range of safety factor, q ($=rB_\phi/RB_\theta$), typically between 0.6 to 3.5. The complete design and engineering considerations for Tokapole II are presented in detail elsewhere [2,3]. Only the general machine description, the changes due to the upgrade, and details specific to the experimental results will be given.

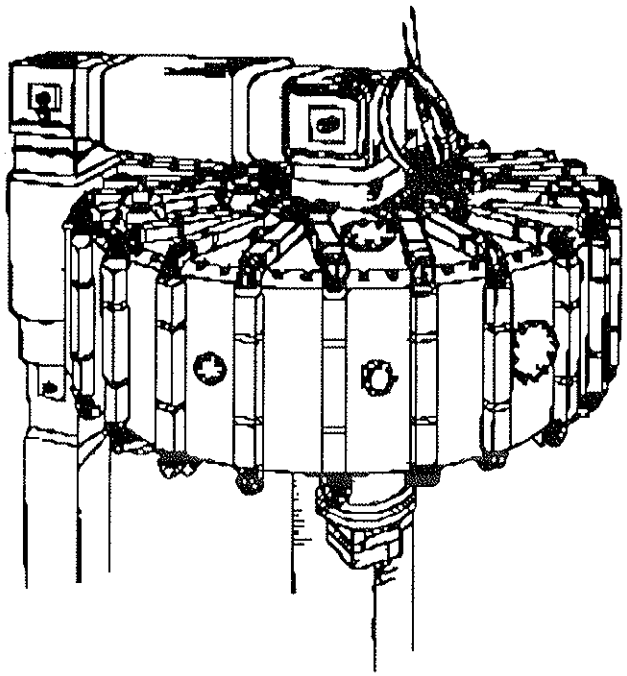

Figure 3.1 The Tokapole II Tokamak

3.1.1 The vacuum vessel

The vacuum vessel for the Tokapole II tokamak (Figure 3.2) has a 44 cm x 44 cm square cross section torus with a 50 cm major radius. The walls are made from 3 cm thick aluminum and have a toroidal and poloidal gap to allow penetration of the magnetic fields into the machine. The poloidal divertor configuration is created by four solid chromium copper rings which are supported by three Inconel rods strapped to each of the rings[4]. The installation of the Inconel supports to replace the old beryllium copper supports was one of the major goals of the Tokapole II upgrade in 1987.

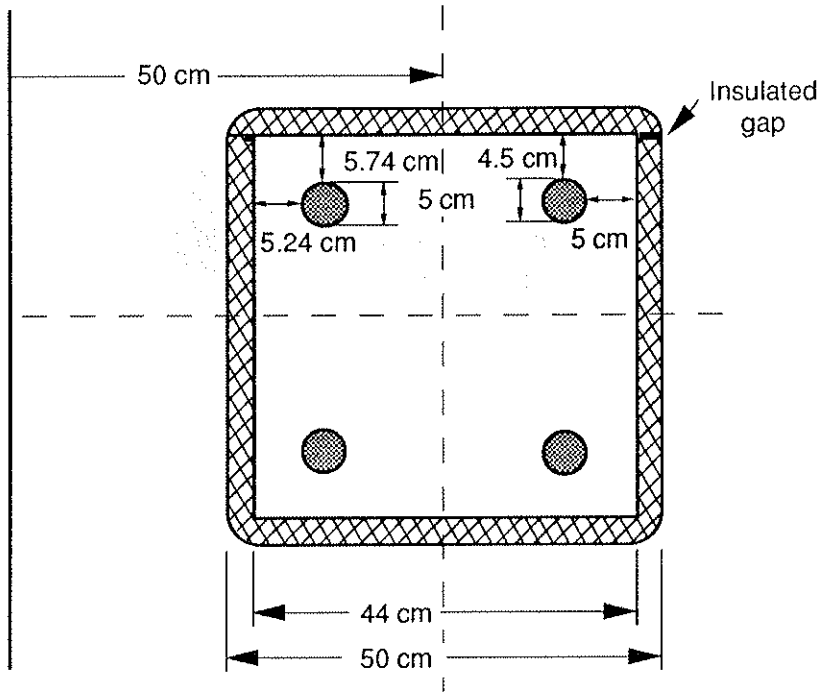

Figure 3.2: Cross-section of the Tokapole II Tokamak

The primary pumping for the vacuum is provided by a 1500 l/sec turbo-molecular pump built by Sargent-Welch. This provides a mid 10^{-7} torr base pressure. Additional pumping can be obtained by titanium gettering of the walls through the use of one or two titanium sublimators. Vacuum conditions are monitored with a quadrupole residual gas analyzer.

Diagnostic access is achieved through various portholes in the vacuum vessel. The majority of the diagnostic access is through $1^1/_2$ inch ports with probe assemblies that have the capability of swivelling 25° with respect to the wall. There are four 4 inch ports through which larger diagnostics can be inserted. There are four six inch ports of which one is permanently dedicated to the turbo-molecular pump.

3.1.2 The toroidal field system

The toroidal field is created by 96 turns of 4/0 wire wrapped around the vacuum vessel. Care was taken to wind the turns so that they would cross the toroidal gap uniformly to reduce the field errors generated inside the vessel. Driving the toroidal field windings is an 0.078 F, 5 kV capacitor bank. The toroidal field bank represents the other major difference between the Tokapole II before and after the 1987 upgrade. As well as a major overhaul of the entire capacitor bank and power delivery systems, 0.024 F was added to the toroidal field circuit to achieve the present total. The toroidal field bank was also reconfigured to form a two

section pulse forming network (Fig. 3.3) in order to produce a "flat" toroidal field for about 12 to 15 msec. This was accomplished by the installation of a 640 μH inductor in the circuit as shown in Fig. 3.3. The bank is switched using a class E ignitron. The bank is also passively crowbarred after peak field by a second class E ignitron to prevent the capacitors from reversing their voltages.

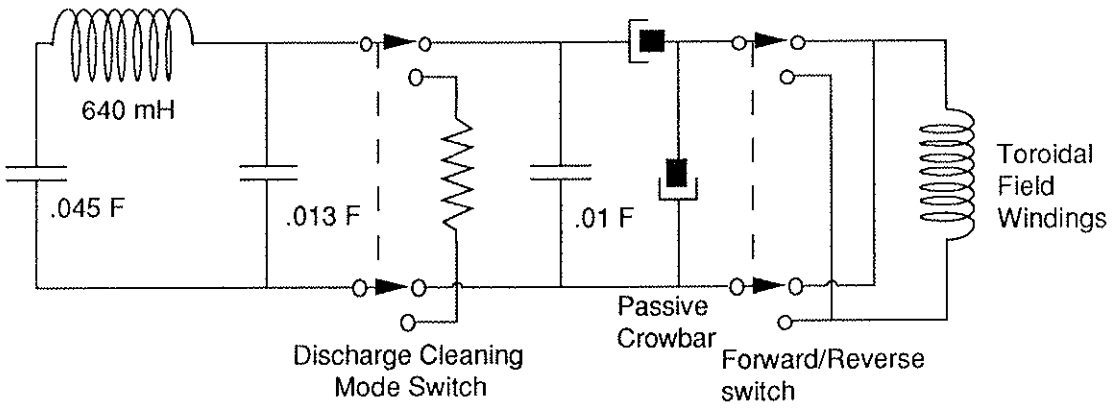

Fig 3.3 Toroidal Field Circuit

The bulk of the toroidal field bank is switched out of the circuit during the rapid discharge cleaning of the Tokapole II tokamak. This is accomplished by a pneumatically controlled knife switch. The rapid discharge cleaning is typically done before running normal discharges to condition the walls and any probes in the tokamak.

3.1.3 The Poloidal Field System

The poloidal field is generated by four internal chromium–copper rings inductively driven by a 0.17 V-s iron core. The primary windings

consist of 80 total turns of two gauge wire wrapped around the iron core. The primary turns are wound such that the poloidal system can be run with either a 40:1 turns ratio (normal mode) or an 80:1 turns ratio. The power supply for the poloidal field system is a 0.0075 F, 5kV capacitor bank. The poloidal field system (Fig. 3.4) can be either passively crowbarred or actively crowbarred with an 0.96 F, 450V electrolytic capacitor bank.

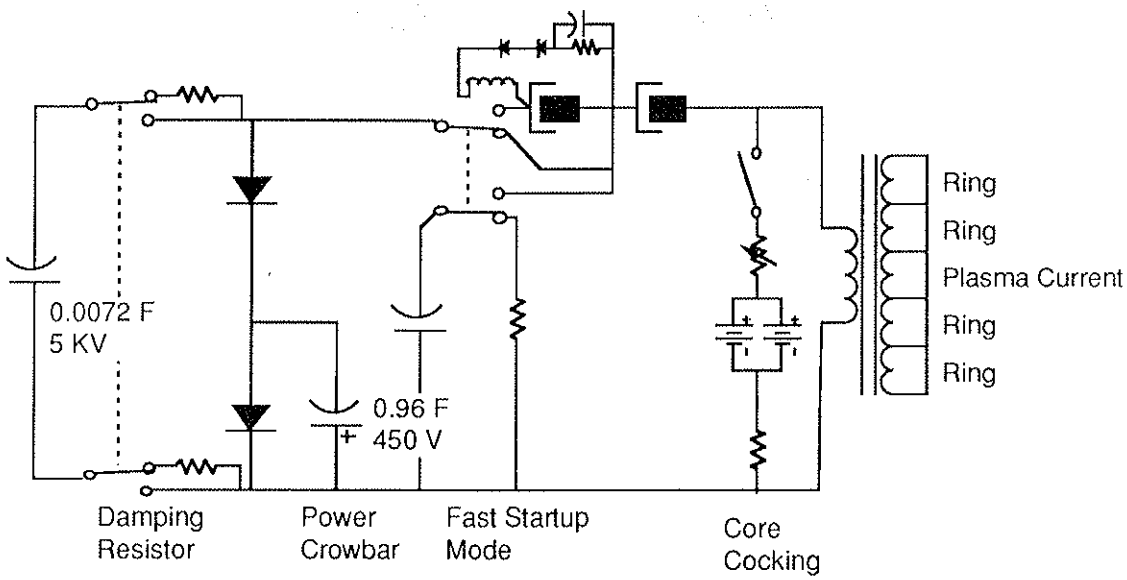

Figure 3.4 Poloidal Field Circuit

The field configuration obtained by the internal rings in the absence of the plasma current is an octupole field (Fig. 3.5a). The plasma current changes the flux plot (Fig. 3.5b) to form distinct regions of common flux (the flux lines encircling all of the currents) and private flux (flux lines enclosing only one current). The region where the magnetic field lines encircle all of the current carriers is called the common flux region. The region in which field lines encircle only one

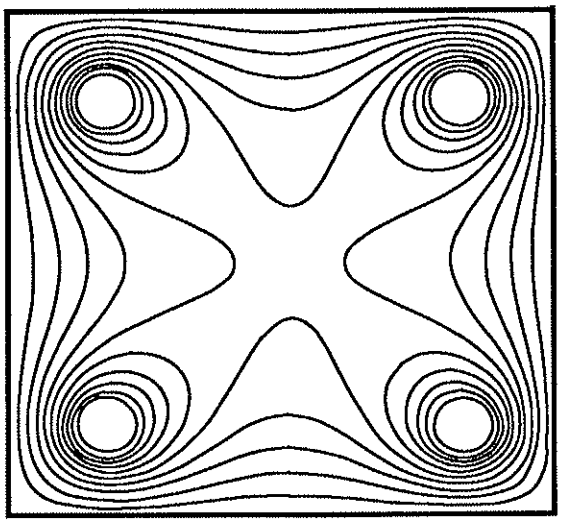

Figure 3.5a Poloidal flux plot for the case with no plasma current

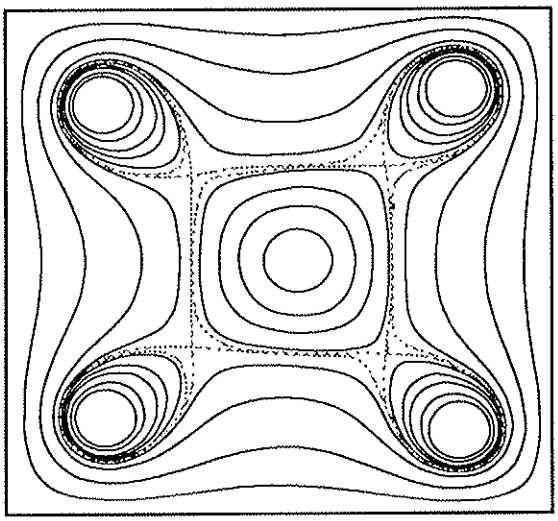

Figure 3.5b Poloidal flux plot showing the typical location of the separatrix (indicated by the shaded line)

current carrier is known as the private flux region.

The regions are separated by field lines known as separatrices. Under normal circumstances the separatrices are degenerate and are collectively known as the separatrix. The location of the separatrix is considered the edge of the plasma, and as such all measurements made inside the plasma refer to positions within the separatrix and all measurements made in the edge or outside the plasma refer to positions outside the separatrix and in the common flux region. The plasma current resides mainly in the central flux region[5–8] which is called the current channel.

3.1.4 General Operating Parameters

Detailed characteristics of the operating parameters can be found in previous works.[6-8] Only a cursory discussion of the equilibrium properties will be presented here. For the data presented in this thesis, the Tokapole was operated in several parameter regimes. The regimes are distinguished by their effective edge safety factor which ranged from $q_a = 0.7$ to $q_a = 3.5$. The lower safety factors were achieved by lowering of the toroidal field and the increasing the poloidal gap voltage to drive more plasma current.

Because of the unusual nature of the Tokapole II tokamak, these q_a's represent the effective edge safety factor of a cylindrical plasma with the same plasma current as that contained within the divertor separtrix. Details of the models and assumptions used in the following equilibrium

calculations can be found in the references.[9] q_a is calculated by estimating the plasma radius, in centimeters, via

$$a = 17.3\,|I_P/(I_H + I_P)|^{1/4} \qquad (3-1)$$

where I_p is the plasma current and I_H is the total ring current both in kAmps. The estimate is then

$$q_a = 10^{-4}\, a^2 B_T / I_P \qquad (3-2)$$

where B_T is in kgauss.

The energy confinement time is estimated as a global quantity. This is due to the lack of the profiles necessary to calculate the confinement from insatability models. The estimate of the global confinement time is given by τ_E = stored energy/input power. The stored energy used for this estimate is the kinetic energy of the plasma given by the product of the density and the temperature. Since the Tokapole II has no appreciable auxillary heating, the input power is given by the ohmic input power. To get the global estimates for these quantities, several intermediate quantities need to be calculated.

First, an estimate of the loop voltage, in volts, is

$$V_l = \frac{1}{2}(1 + t/75)V_{pg} + 0.0045(1 - t/37)I_H - 2.3\dot{I}_p/\sqrt{a} \qquad (3-3)$$

where V_{pg} is the measured poloidal gap voltage and t is in msec. From

this the ohmic input power is given, in kwatts, simply by

$$P_{OH} = I_P V_l \qquad (3-4)$$

The calculation of the conductivity temperature assumes Spitzer resistivity, effective ion charge of one, and a uniform current distribution. The temperature, in eV, is then given by

$$T_e = 376\left(|I_P/V_l|/a2\right)^{2/3} \qquad (3-5)$$

The final quantity necessary to estimate the confinement time is the density. A Langmuir probe is located between the upper outer ring and the wall. Using the relation $J_{sat} \alpha n_e\sqrt{T_e}$,the average density is calculated by

$$\langle n_e \rangle = \frac{0.05 J_{sat}}{\sqrt{T_e}\,(1 - exp(-45/T_e))} \qquad (3-6)$$

with units of 10^{12} /cm^3. The factor, $(1 - exp(-45/T_e))$, is a correction due to the use of only a 45 V bias on the probe. The factor of 0.05 includes a correction which makes the probe measurement of the density agree with the line averaged density as measured by a microwave interferometer.

Finally, the electron energy confinement time is given, in milliseconds, by

$$\tau_E = \frac{0.144\langle n_e \rangle T_e}{P_{OH}} \qquad (3-6)$$

This is the quantity which will be referred to when estimates of the global confinement are used.

The working gas for all of the discharges was hydrogen. The hydrogen was puffed into the vacuum vessel 16.66 msec before the poloidal field circuit by the use of a fast piezoelectric valve. The toroidal field was triggered 9 msec before the poloidal field to insure that the discharge takes place over an interval of constant toroidal field. The digitizers were triggered at various times during the discharge. The relative timings are illustrated in Figure 3.6.

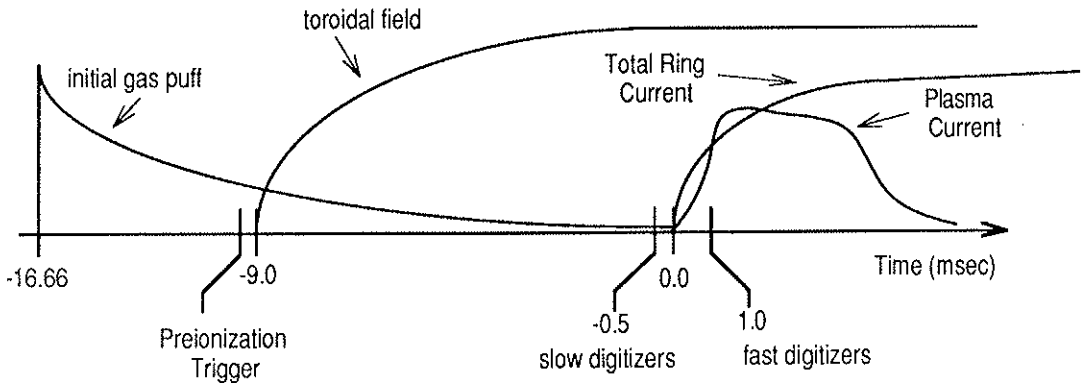

Figure 3.6 Relative timings used to create the discharges. Generic waveforms are shown for illustration purposes.

The discharge characteristics depended on the turns ratio of the primary windings used and the capacitor bank settings. For the lower q_a discharges the primary windings for the poloidal field were run with a 40:1 turns ratio. The higher q_a discharges were run with both 40:1 and 80:1 turns ratios.

The lower q_a discharges ($0.7 \leq q_a \leq 1.5$) had behavior similar to that

of Figure 3.7. These discharges were relatively short and not well confined (τ_E < 100 μsec, where τ_E {= Total Energy/Input Power} is the estimated global energy confinement time). The interval for which there was an approximate equilibrium is indicated in Figure 3.7. This interval was of comparatively short duration so that averaging had to be done over many similar shots.

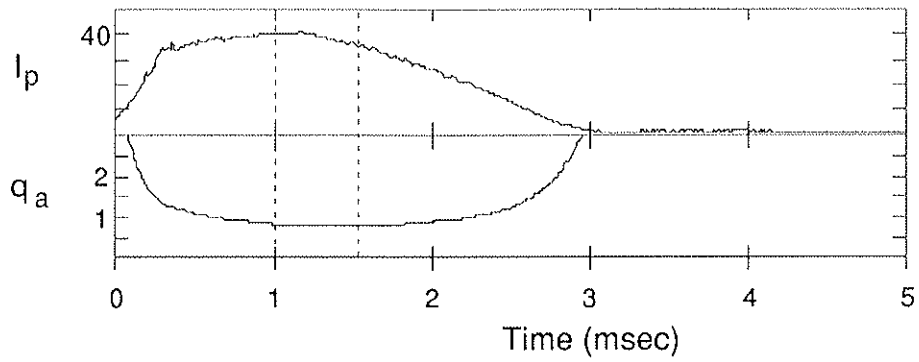

Figure 3.7 A typical q = 0.7 shot showing the plasma current, "effective edge q". All data for the statictical ensembles was taken in the region indicated.

The higher q_a discharges ($1.5 \leq q_a$) at the 40:1 turns ratio were similar to that of Figure 3.8. The initial part of the discharge is similar for all 40:1 discharges however there develops a plateau which can extend several milliseconds past the initial current phase. Although the plateau had the best equilibrium properties ($\tau_E \geq 100$ μsec), it suffered

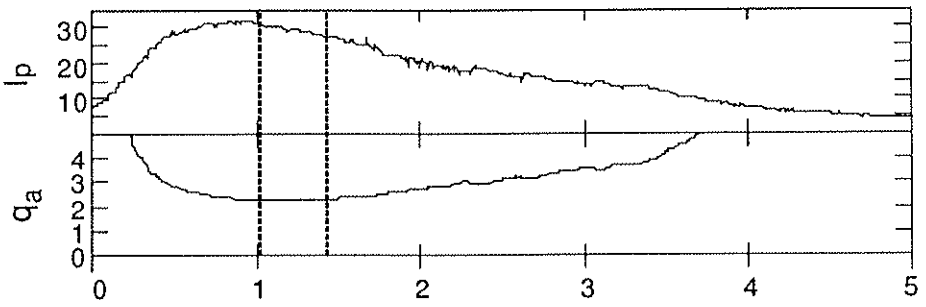

Figure 3.8 A q=2.5 discharge showing the plasma current and the effective edge q. The region between the dashed lines indicates whenthe data was taken for the ensembles.

from excessive MHD activity (evidenced by the soft x-ray signals) which would dominate the background fluctuations and turbulence. Due to extreme difficulty in finding suitable records in this plateau the data for these discharges was taken at peak current as was done with the lower q_a discharges.

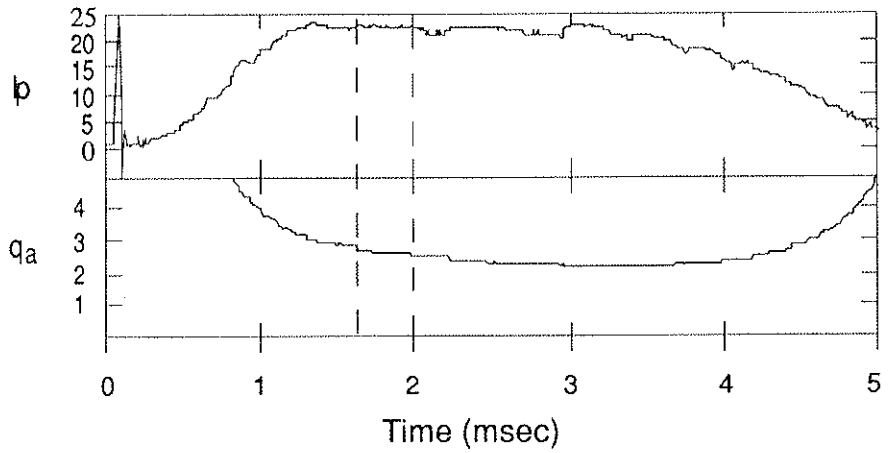

Figure 3.9 Typical discharge for a q_a = 2.2 plasma with the primary turns ratio of 80:1. The region indicated by the dashed lines is where the ensembles were taken for the statistical averages.

The higher q_a discharges with the 80:1 turns ratio on the primary windings are shown in Figure 3.9. The plasma current reached a plateau which lasted for several milliseconds. The MHD activity starts late in the plateau so finding appropriate data records was much simpler.

3.2 General Diagnostics

Several diagnostics are used to monitor the general character of the plasma discharges in the Tokapole II tokamak. Only those diagnostics actually used in the analysis of the discharges used in this thesis will be described.

A 70 GHz interferometer was used to measure the line averaged density on the midcylinder of the machine. The circuit used to detect the fringe shifts[10] caused some noise problems on the high frequency magnetic diagnostics and hence was not used for the time that the fluctuation data were taken. The interferometer was used to determine the densities just before and immediately after a given data run to check the reproducibility of the discharges.

Several optical diagnostics were used to determine the discharge quality and relative temperature. A set of filtered photomultiplier tubes was used to monitor radiation lines from O III, C III, Cu I and N III. The oxygen and the carbon are predominately to monitor hydrocarbon impurities. The nitrogen is primarily from either air leaks, if they exist on the machine, or from the bombardment of the boron nitride probe

sheaths which are used as a heat and particle shield for many of the probes. The copper gives a measure of how much the plasma is interacting with the internal rings.

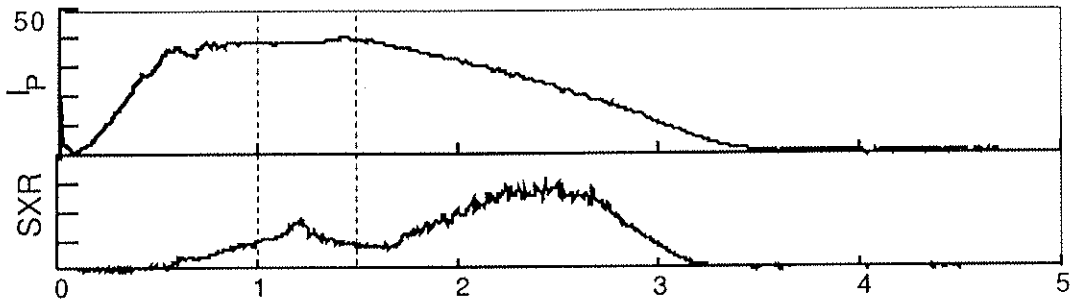

Figure 3.10 Central chord soft x–ray for a q=0.8 discharge with a primary turns ratio of 40:1. The dashed lines indicate the time interval over which the time records to be analyzed were selected.

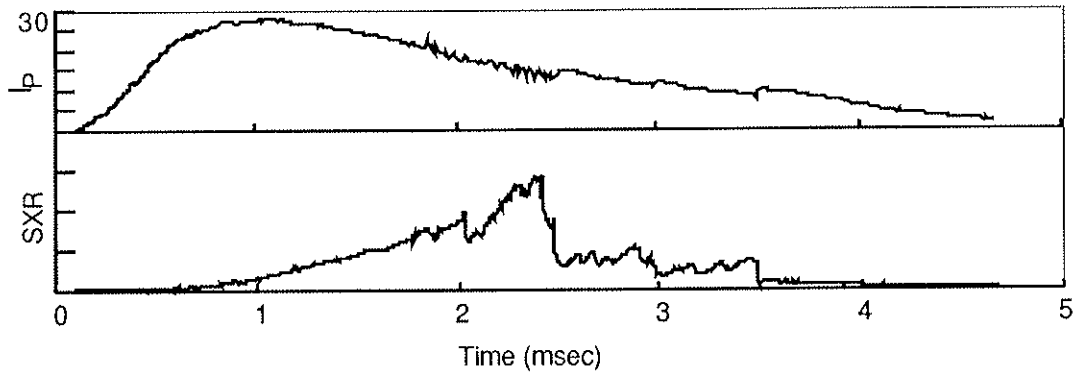

Figure 3.11 Central chord soft x–ray for a q=2.0 discharge with a primary turns ratio of 40:1. The dashed lines indicate the interval over which the data was recorded.

A set of seven filtered surface barrier detectors comprise a vertical array used to measure the soft X-ray emission between 60 eV and 300 eV. The structure of the emission gives approximate locations for the sawteeth inversion radii and hence approximate locations for the

appropriate rational q surfaces supporting the disruptive modes[7,8,11]. Figures 3.10, 3.11, and 3.12 show typical central cord soft x–ray signals for similar types of discharges as mentioned earlier.

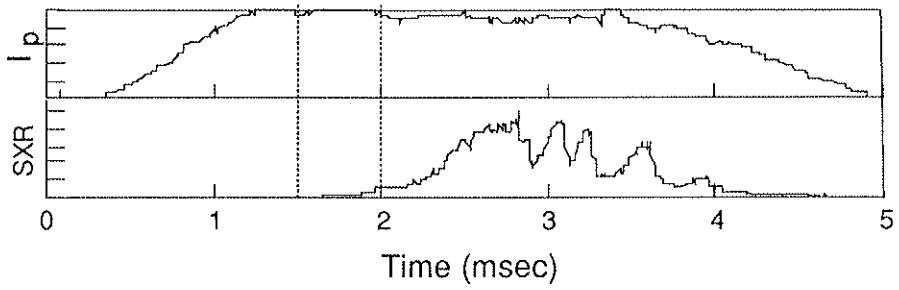

Figure 3.12 Central chord soft x-ray for a q =2.8 discharge with a primary turns ratio of 80:1. The dashed lines indicate the interval over which the data was analysed.

3.3 Magnetic Pickup Coils and Electronics

The experimental results were obtained using magnetic pickup coils and specialized electronics. The diagnostic is unique and deserves some detailed discussion.

3.3.1 Magnetic Pickup Coils

All the magnetic pickup coils used in this thesis were built in house. Two main type of coils were used, designated *large coils* and *small* or *mini coils*. Several variations of both of these schemes have been used to obtain the data. Although the general structure of the two schemes is

the same, construction techniques and how perturbing the probe is to the plasmas are significantly different.

The large probes (Fig 3.13a) consist of a 1/4" O.D. stainless steel sheath with 0.0625" thick walls for the bulk of the probe. The end which is inserted into the plasma consists of a 1/8" I.D., 0.006" thick wall stainless tube which is capped and vacuum soldered to the 1/4" stainless tube. The 1/8" tube then has a boron nitride sheath glued to it with Sauereisen 29 binder. The boron nitride serves as a particle shield from the plasma. Since this assembly serves as both a vacuum and particle shield, the magnetic coil assemblies can be inserted inside the tubes without breaking the vacuum.

One advantage of this scheme is that once the probe is inserted, the coils can be moved radially without moving the sheath. This ensures that the plasmas are seeing the same "obstructions" for the entire profile. A major disadvantage is that at the higher frequencies (above a few hundred kilohertz) the shield begins to phase shift the $\dot{B}$ signals due to skin effects of the stainless steel.[13] Also the large probes can usually only be inserted to about 6 cm from the geometric axis before they start to significantly perturb the gobal discharge characterics.

Two types of mini-probes, distinguished by the material used for their particle shield, were used in this thesis. The mini-probes were originally designed by Prof. R. N. Dexter and developed by I. H. Tan and J. A. Goetz for other experiments on Tokapole II. The mini probes were designed to allow penetration of a probe into discharges with higher edge q's. To some degree this was successful in that the mini-probes

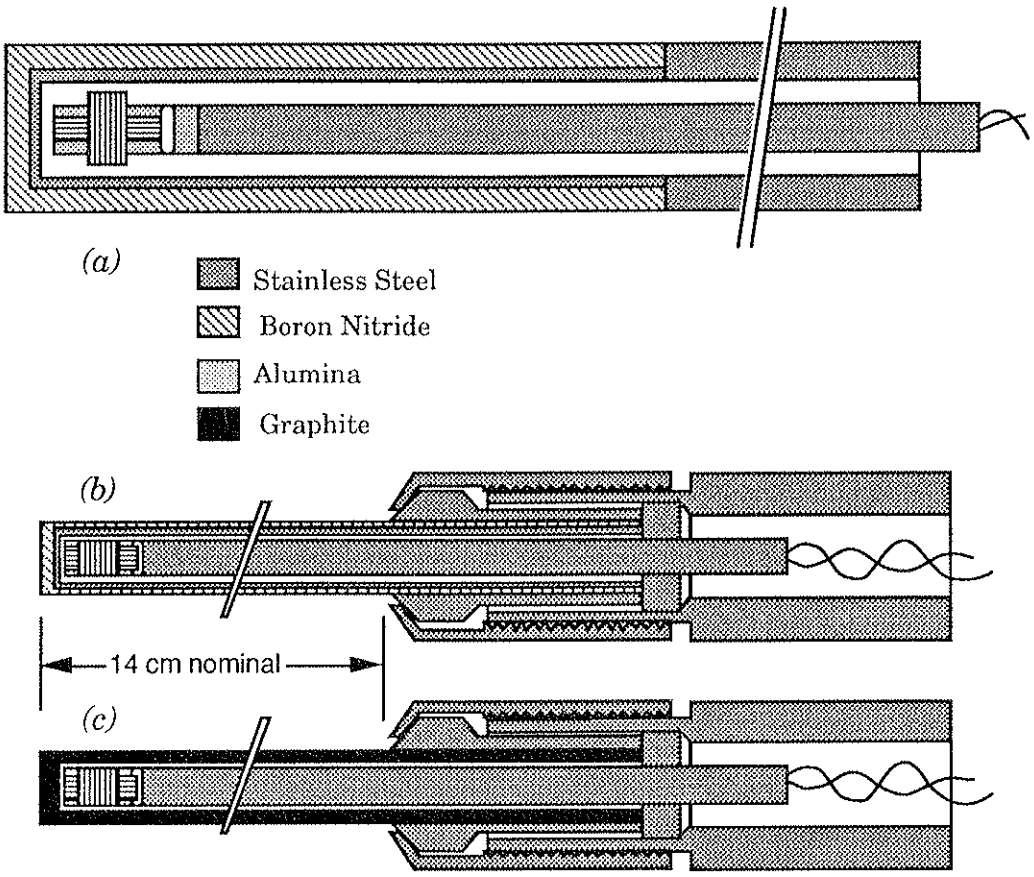

Figure 3.13 Relative size and construction of the magnetic probes used in this thesis. The major difference, other than size, is that the large (1/4") probe in (a) and the original mini probes shown in (b) have a thin stainless shield used to reduce electrostatic pickup by the coils. The graphite clad mini probe in (c) has a much better frequency response due to the higher resistivity of the graphite. For both (b) and (c) the nominal O.D. is 0.100".

could be inserted to about x=4 cm from the machine axis without any noticeable degradation of either the global characteristics of the discharges or the magnetic fluctuations outside the separatrix (Fig 3.14). From x=4 cm to the center the global characteristics and the

edge magnetic fluctuations below 300 kHz were unchanged, but the edge magnetic fluctuations above 500 kHz completely decorrelate as the mini-probe is inserted to the center of the machine.

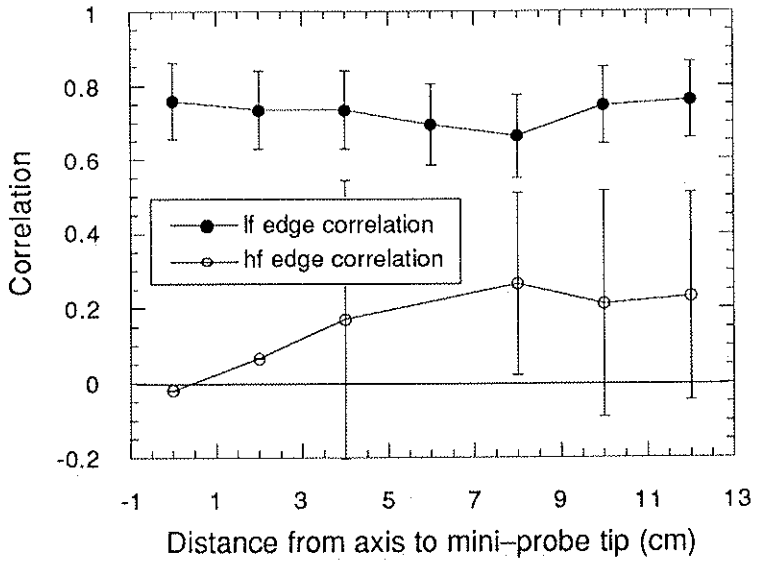

Figure 3.14 *Correlations between radially separated coils in the edge region show the effect of the mini–probe insertion on the radial fluctuations in a q_a = 1.3 discharge. For low frequencies (10–500 kHz at x=13 and 15 cm) no effect is seen on the edge fluctuations. At high frequencies (0.5–2 MHz at x=12 and 14 cm) the edge fluctuations decorrelate when the mini–probe reaches the center of the machine.*

The first mini-probes had stainless steel electrostatic shields surrounded by boron nitride particle shields (Fig 3.13b). Although these probes could be inserted farther into the discharge, they still suffered

from phase shift at the higher frequencies. Because the vacuum seal was made at the end of the probe outside the machine the coil was not movable within the sheath. Thus to make a radial profile required the moving of the entire probe. From x=4 cm from the machine axis to the edge this did not seem to pose a problem with irreproducible discharges. Inside of x=4 cm, because the edge fluctuations at the higher frequencies did change, it is not realistic to assume that the plasmas were reproducible. For edge q's below about 1.4 there was little if any effect of the probes on the global characteristics of the discharges.

The next generation of mini probes (Fig 3.13c) were similar in size but did not have a stainless steel electrostatic shield. Instead they had a graphite particle shield which also served as the electrostatic shield. Because of the higher resistivity the graphite probes did not suffer from phase shift at the highest frequencies used. The graphite probes did not otherwise improve the ability to move the probe into the discharge over the boron nitride clad probes.

A specialized probe, referred to as the *forked* probe was used to make the phase and k spectra measurements used in this thesis. The forked probe (Fig 3.15) consisted of three graphite clad mini probes mounted so as to have the radial coils co-linear and the transverse pickup coils co-planar.

3.3.2 Amplifiers and Filters

Due to the small signal level from the magnetic pickup coils the

output from the probes was amplified and filtered. There are two major frequency regimes covered in this thesis: 10 kHz $\leq f \leq$ 500 kHz (referred to in this thesis as *low frequency*) and 500 kHz $\leq f \leq$ 5 MHz (referred to as *high frequency*).

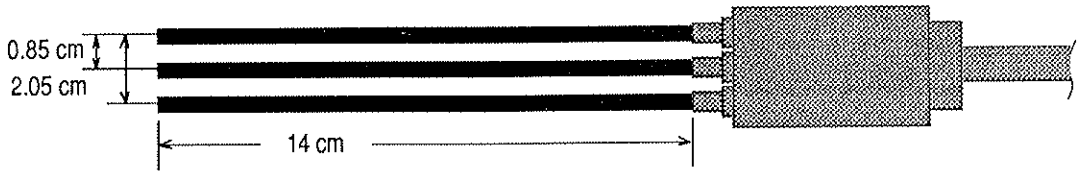

Figure 3.15 Schematic of the "forked"probe. Each tine is a graphite clad mini probe which is held in place by the structure at the right. The requirement on probe length is so that the stainless support structure be well outside of the current channel when the coils at the end of the probe are at the center of the machine.

For the low frequency regime the signals were amplified using a Tektronix AM502 differential amplifier. This amplifier allowed gains from 1 to 5000 with the capability of putting a single pole filter on either the high or low end of the frequency band. Except when noted, all of the low frequency data used an AM502 set with the highpass corner at 10 kHz and the lowpass corner at 1 MHz.

For frequencies above 500 kHz the signals were amplified using an amplifier designed and built in house by D. Kortbawi[14] and T. Lovell. The amplifier has a fixed gain of 66 dB and a 150 Ω attenuator pad which can add 0 to 31 dB of attenuation. This method has the advantage of being able to optimize the amplifier response due to the fixed gain and still obtain various dynamic ranges without detuning the amplifier.

The filters used with the high frequency amplifiers were n = 3 Cauer

elliptic bandpass filters[15,16]. The Cauer elliptic filters were chosen primarily for their sharp rolloff characteristics and large attenuation in the stop bands for a fairly low order filter. The major drawback is the nonlinear phase response of the filter especially near the corners. A detailed phase calibration for each probe, amplifier and filter combination was required in order to measure properly the relative phase between two probes.

3.3.3 Calibration of the Magnetic Probes

The absolute calibration of the magnetic probes for both amplitude and phase response was done utilizing two sets of Helmholtz coils. For frequencies below 500 kHz a multiturn Helmholtz coil set which generated 0.056 Gauss/amp was used. The response versus frequency was recorded and, for cases where the response is linear, an effective area was determined for the coil. For the multicoil sets the relative phase between coil/amplifier sets was determined to be either zero or sufficiently close to zero as not to pose a problem.

The high frequency response of the coil/amplifier/filter sets was measured using a Helmholtz coil set built specifically for calibrations between $0.5 \leq f \leq 5.0$ MHz. Because of differences in construction of the amplifier/filter sets, amplitude and phase calibrations must be applied in frequency space.

3.4 Data Acquisition System

Once the signals have been amplified and filtered, the signals were then digitized by commercially available transient recorders. The plasma current, line averaged density, ion saturation current, poloidal gap voltage and toroidal field on axis were recorded at 100 kHz sampling rate with a DSP Technologies TRAQ system model 4012 controller with a model 2812 transient recorder and a model 8800 memory module. The array of soft x-ray detectors and the impurity signals were digitized at 500 kHz sampling rate with either a DSP Technologies TRAQ system model 4012A controller with a model 2810 transient recorder and a model 8800 memory module or a LeCroy model 8210 transient recorder with a model 8800/10 memory module.

The signals from the magnetic pickup coils were recorded using several transient recorders. For the frequency range $10\ \text{kHz} \leq f \leq 300\ \text{kHz}$, the magnetic signals were recorded at 1 MHz sampling rate using a LeCroy model 8210 transient recorder with a model 8800/10 memory module. For the frequency ranges above 300 kHz the magnetic signals were recorded at either 10 MHz or 20 MHz sampling rates using a DSP model 2001A transient recorder.

The software used for managing the CAMAC was the Model Data System (MDS) developed at the Massachusetts Institute of Technology and run on a MicroVAX II. The software for analyzing the data utilized the Interactive Data Language (IDL) from Research Systems Inc. and VAXFORTRAN. All of the programs for doing the analysis used in this

thesis were developed in house with the aid of many former and current graduate students and undergraduate hourlies. Details of the techniques used for the analysis can be found in the appendices.

References

[1]A.P. Biddle, R.N. Dexter, R.J. Groebner, D.T. Holly, B. Lipschultz, M.W. Phillips, S.C. Prager, and J.C. Sprott, Nucl. Fusion **9**, 1509 (1979)

[2]J.C. Sprott and T.W. Lovell, University of Wisconsin-Madison PLP 744 (1978)

[3]R.J. Groebner, Ph.D. Thesis, *Vacuum Ultraviolet Spectroscopic Study of Plasma Impurities in the Tokapole II Poloidal Divertor Tokamak*, University of Wisconsin-Madison (1979)

[4]J.C. Sprott, University of Wisconsin - PLP 962 (1985)

[5]Eijiro Uchimoto, PhD Thesis, *Numerical Simulations of Resistive Magnetohydrodynamic Instabilities in a Poloidal Divertor Tokamak*, University of Wisconsin-Madison (1988)

[6]N. S. Brickhouse, *et al,* in *Prodeedings of the Tenth International Conference on Plasma Physics and Controlled Nuclear Fusion Research,* London, 1984 (IAEA, Vienna, 1985) 385

[7]T.H. Osborne, PhD thesis, *Disruptive Instabilities in a Poloidal Divertor Tokamak*, University of Wisconsin-Madison (1984)

[8]Richard Moyer, PhD thesis, *Magnetic and Material Limiter Discharges in Tokapole II*, University of Wisconsin-Madison (1988)

[9]J.C. Sprott, University of Wisconsin-Madison,PLP 889 (1983); J.S. Sarff, University of Wisconsin-Madison, PLP 1003 (1987)

[10]H.R. Garner, University of Wisconsin - Madison, PLP 833 (1980)

[11]J.A. Goetz,*Total Magnetic Reconnection During a Tokamak Major Disruption*, submitted to Physical Review Letters

[12]See for example J. D. Jackson, *Classical Electrodynamics, 2nd edition,* John Wiley & Sons, New York (1975) pp 296-298,334-339

[13]D. Kortbawi, PhD Thesis, *Alfvén Wave Studies on a Tokamak*, University of Wisconsin-Madison (1988)

[14]A.B. Williams, *Electronic Filter Design Handbook*,McGraw–Hill Book Company, New York (1981)

[15]A.I. Zverev, *Handbook of Filter Synthesis*,John Wiley & Sons, New York (1967)

Chapter 4: Magnetic Turbulence on Tokapole II

This chapter presents the measurements of magnetic fluctuations on the Tokapole II tokamak. The chapter is divided into three sections. First, there is a description of the magnetic fluctuations in the high frequency (500 kHz $\leq f \leq$ 2 MHz) regime. Comparisons with previous measurements done at low frequency[1] (10–400 kHz) are made. The second section presents the measurements of the parallel correlation and coherence lengths of the radial and poloidal magnetic fluctuations. The third section discusses the results obtained in terms of various fluctuation or transport theories. Where possible estimates of transport quantities are calculated.

4.1 High Frequency (500 kHz $\leq f \leq$ 2 MHz) Fluctuations

The measured magnetic signals at the higher frequencies consisted of two relatively distinct parts (Fig 4.1). There is a quiescent turbulent level which is associated with the broadband magnetic fluctuations in the plasma, and bursts of signal which can be several orders of magnitude higher than the quiescent level. Although it is the quiescent fluctuation level which is the focus of these experiments, a few words should be said about the bursts.

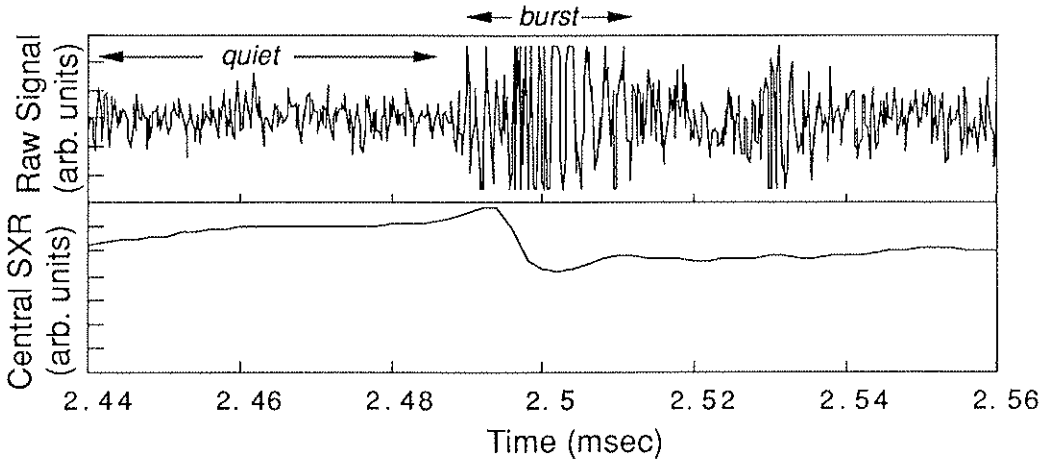

Figure 4.1 *An expanded view of the first soft x-ray crash for shot #4900 from 6 April 1990 shows how rapidly the burst amplitude rises. The burst amplitude can be up to four orders of magnitude larger than during the quiescent parts of the discharge. The burst in this figure was clipped by the transient recorder used to digitize the signal.*

The bursts of activity on the high frequency signals have been correlated with crashes of the soft X-ray signal. There is sometimes evidence of precursor activity at the higher frequencies. The magnitude of the bursts in the frequency range 0.5 – 5.0 MHz can be up to four orders of magnitude larger than the quiescent fluctuation level. The duration of the bursts is typically less than 100 μseconds. For comparison a low frequency (10 – 500 kHz) magnetic signal is shown in Figure 4.2. The low frequency fluctuations also exhibit the bursts of activity, but the increase in amplitude is usually two orders of magnitude or less. Due to the extreme transient nature of the bursts, stationarity cannot be assumed. Thus, many of the usual spectral analysis techniques can not be applied. The rest of this paper deals

only with the quiescent parts of the signals and no other mention will be made regarding the bursts of activity.

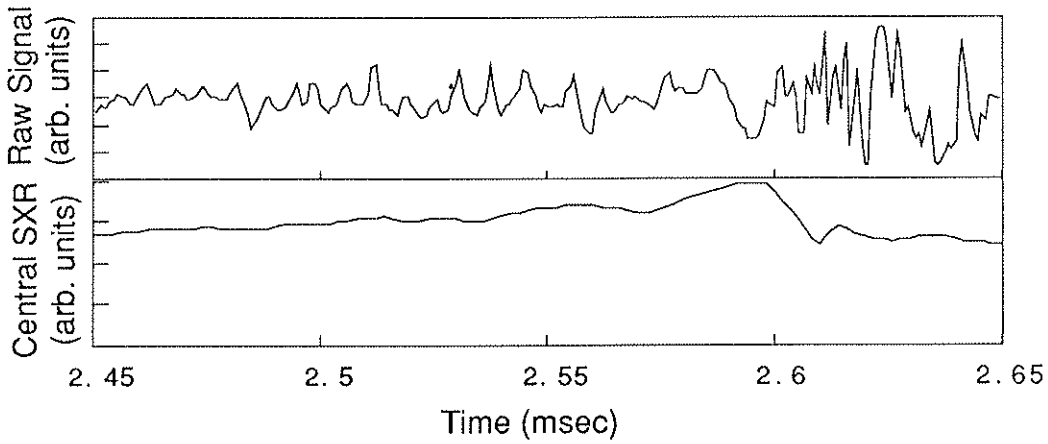

Figure 4.3 The low frequency (10 – 500 kHz) magnetic signals show similar bursts. The amplitude increase is usually less than two orders of magnitude larger than the quiescent fluctuations. Data are from shot #4814 taken on 5 April 1990.

4.1.1 Amplitudes and scaling of the high frequency fluctuations

Figure 4.4 shows the fluctuation amplitude over the frequency interval 0.5 to 2.0 MHz at various effective edge q's (hereafter denoted by q_a). The magnetic pickup coil, in a 1/4" probe sheath, was kept on the midplane at a radius seven centimeters from the geometric center of the machine. The amplitude of the fluctuations decreases over three orders of magnitude as q_a is increased by more than a factor of four. As much as possible the total plasma current was kept the same in order to distinguish the effects due to the edge q from those due to the plasma current.

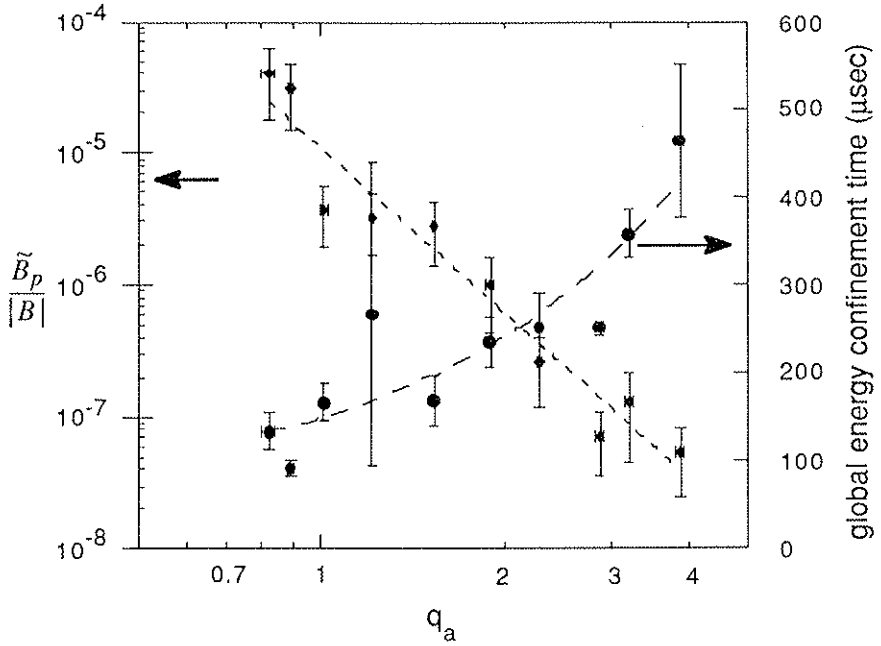

Figure 4.3 Normalized fluctuation level and global confinement time as a function of q_a. Fluctuation data are from a 1/4" probe at x=7 cm along the midplane and are over the frequency range 0.5 to 2.0 MHz.

Three values of total plasma current (40 kA for $q_a < 1.5$, 30 kA for $1.5 < q_a < 2.5$, and 20 kA for $q_a \geq 2.5$) were needed due to machine limitations. If the changes in the plasma current are neglected, a relation between the magnetic fluctuation amplitudes and q_a can be found. Fitting a power law to the data gives the relation

$$\frac{\tilde{B}_p}{|B|} = 1.1\times10^{-5}\, q_a^{-4.1} \qquad (4\text{–}1)$$

The poloidal magnetic fluctuations in the 0.5 – 2.0 MHz range are more sensitive to q_a than the radial magnetic fluctuations in the

100 – 400 kHz range reported by Graessle.[1] There, he found the lower frequency fluctuations scaled as $q_a^{-1.78}$.

Figure 4.4 also shows the global energy confinement time versus q_a for the same discharges. Profiles of the equilibrium quantities necessary to calculate the local transport and confinement are not available for Tokapole II. Thus the confinement is estimated as a global quantity (see section 3.1.4). A direct relation between the magnetic fluctuations and the energy confinement is not determined here.

To determine the effect of the plasma current on the magnetic fluctuation level, a probe in a 1/4" sheath was inserted to x=7 cm into a discharge with q_a=0.7. Three plasma currents (40, 60, and 80 kA) were used while increasing the toroidal field to keep q_a constant. Figure 4.5a shows the fluctuation spectra over the interval 0.5–2.0 MHz. As the current goes from 40 to 60 kA, the bulk of the increased power is between 0.5 and 0.8 MHz with some enhancement above about 1.4 MHz. When the plasma current is increased to 80 kA the fluctuations in the frequency range from 1.2 to 2.0 MHz were increased substantially over the previous two cases. The fluctuation level in the range 0.8 to 1.3 MHz seemed to be relatively insensitive to changes in the plasma current. Figure 4.5b shows the integrated fluctuation power. The curve fit gives the relation

$$\tilde{B}_p = 0.005 I_p^{1.3} \qquad (4-2)$$

This compares favorably with the scaling of $I_p^{3/2}$ found by Graessle[1] for radial magnetic fluctuations. However, due to the errors in the measurements, the scaling is anywhere from q_a^2 to q_a^0.

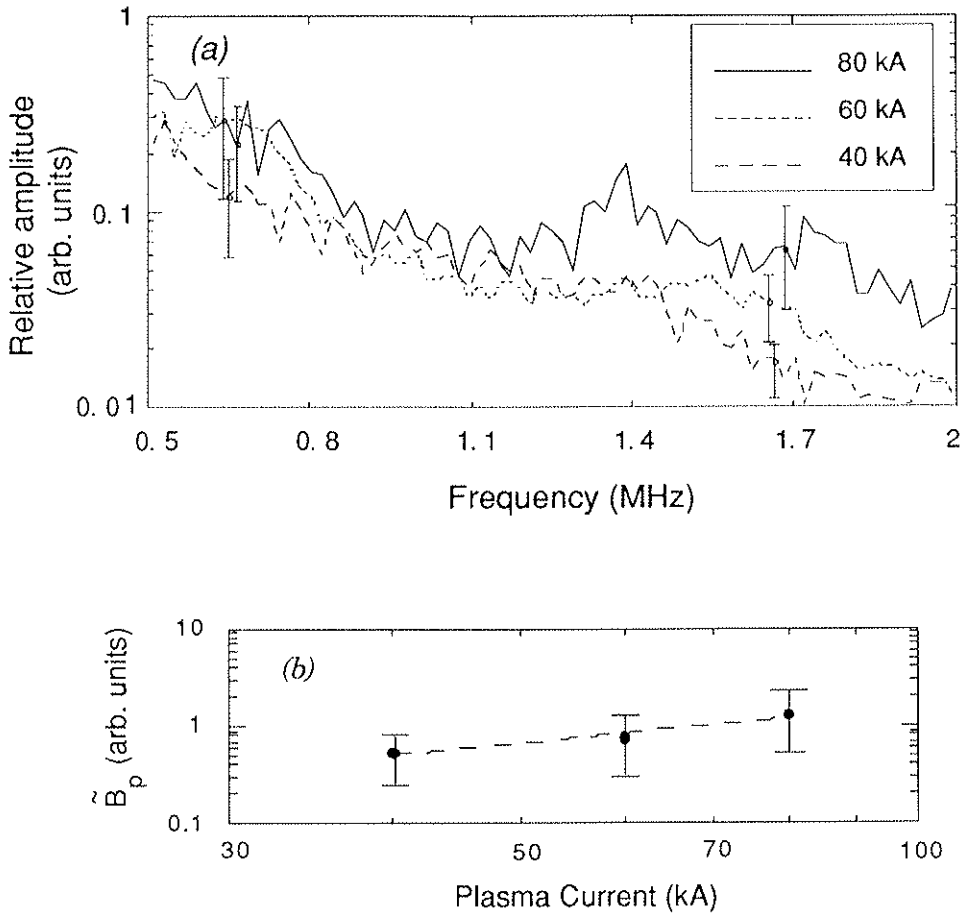

Figure 4.4 *Frequency spectra (a) and fluctuation amplitude (b) for various values of plasma current at q_a=0.7. The probe was at x=7 cm on the midplane and measured poloidal magnetic fluctuations.*

4.1.2 Frequency spectra and profiles

Figure 4.5 shows the spectra for the poloidal fluctuations at various radii in a q_a=0.7 discharge. A 1/4" sheath was placed into the discharge on the midplane and held fixed while the probe was moved within the sheath. A narrowband mode centered at 1.1 MHz is evident on the otherwise featureless spectra. The broadband part of the spectra increases in amplitude as the probe is moved passed the separatrix (at approximately x=9 cm), but the relative shape is insensitive to position.

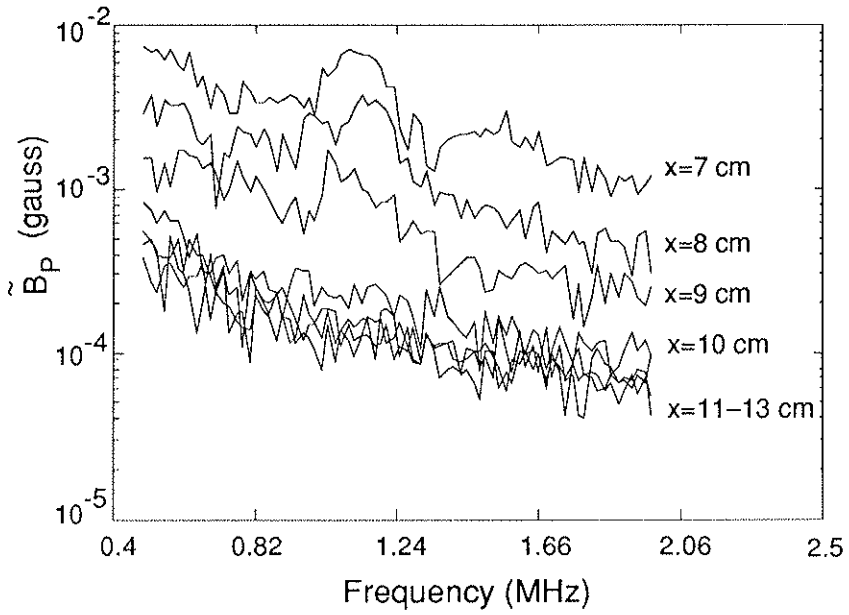

Figure 4.5 Poloidal fluctuation spectra at various radii in a discharge with q_a=0.7 .

The narrowband feature, on the other hand, shows a definite radial structure and seems to be entirely contained within the separatrix. Unfortunately this mode was only present for this one data set and could not be recreated. It could not be determined what had changed to

cause the feature to disappear. For all the data presented in this thesis, this is the only narrowband feature which has been found in the quiescent parts of the magnetic signals at frequencies above 500 kHz.

A similar experiment was performed with q_a=2.0. The spectra were not only featureless for this case,but the fluctuation levels did not change appreciably over the entire radius measured. It has been reported previously that the low frequency magnetic fluctuations tend to follow the equilibrium profiles more so than the gradients. The higher q_a discharges tend to have peaked profiles so the probe may not have been inserted far enough to see the increase in the equilibrium quantities.

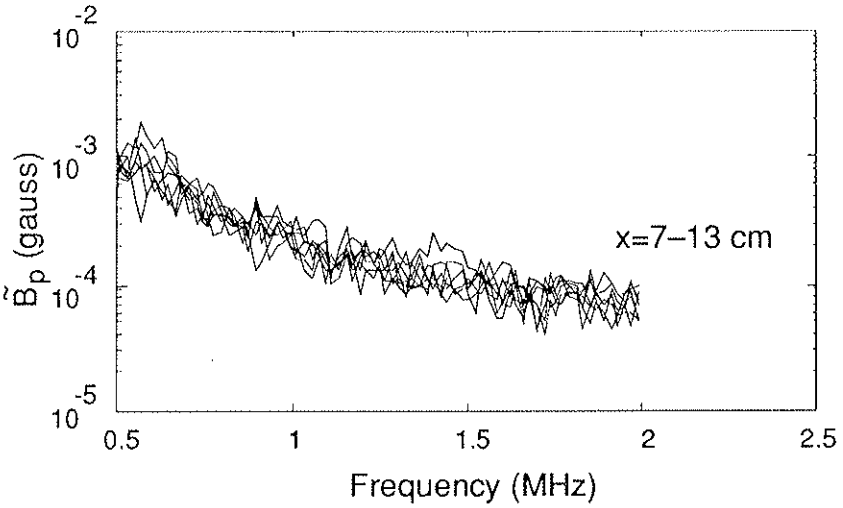

Figure 4.6 Poloidal fluctuation spectra at various radii in a discharge with q_a=2.0.

For comparison purposes, Figure 4.7 shows a low frequency set of spectral profiles taken using a boron nitride clad miniprobe in a q_a=1.3

discharge. The profile shape is similar to that of high frequency fluctuations in the q_a=0.7 discharges. The fluctuations at all radii show the similar featureless spectrum, however the fluctuations at x=5 cm show measurably more power for frequencies above 250 kHz than for all other radii. This location corresponds to the radii where the high frequency edge fluctuations began to decorrelate. Thus this extra power may be related more to a plasma perturbation by the probe than to anything else.

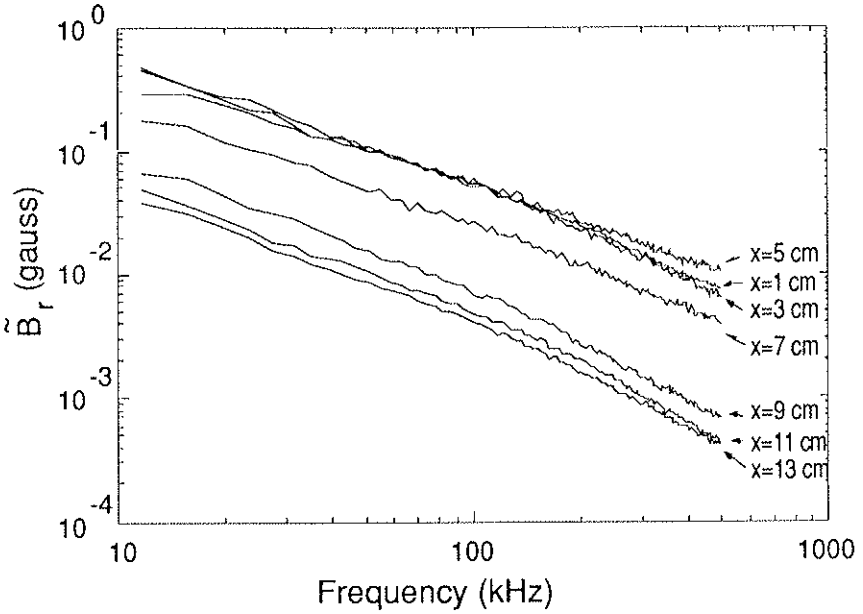

Figure 4.7 Spectra of the radial magnetic fluctuations in the frequency interval 10–500 kHz at various radii.

Figure 4.8 shows the integrated fluctuation profiles normalized to the fluctuation level at x=13 cm. The fluctuations for the lower q_a discharges increase sharply inside the separatrix (located at

approximately 9 cm for $q_a < 1.5$). This is consistent with the fluctuations following the broad equilibrium profiles assumed to exist for the lower q_a discharges. For q_a=2.0 the relatively constant profile may be attributed to the peakedness of the equilibrium profiles.

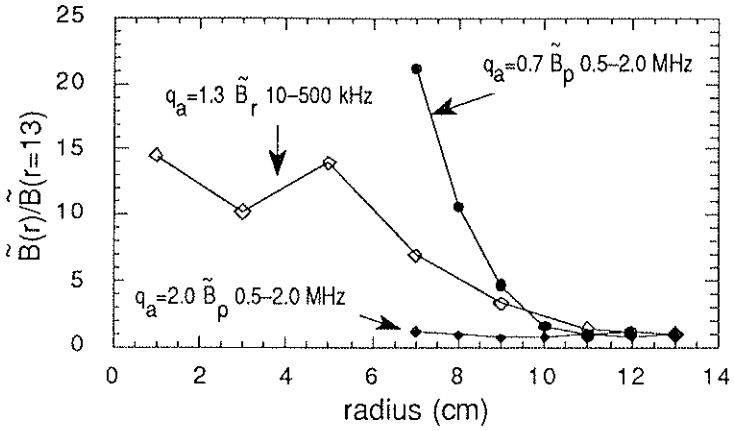

Figure 4.8 Radial profiles of the integrated magnetic fluctuations normalized to the fluctuation level at x=13 cm.

4.2 Correlation and coherence measurements

To determine the spatial characteristics of the turbulence requires the use of multiple probes and some means of prescribing how the fluctuations at one location are related to those at another. Correlation techniques (see appendix A) were used in this thesis to determine what, if any, causal relation exists between the magnetic fluctuations in various parts of the Tokapole II. By measuring the cross-correlations between spatially displaced probes, it can be determined whether signals which are random in time are also random in space.

It should be noted that this method is not foolproof. It is possible,

especially for microturbulence, for several modes with different spatial scales to have the same frequency. For this to happen all that is required is that $k_1 v_1 = \omega = k_2 v_2$,where k_i and v_i are the wavenumber and phase velocity associated with a particular fluctuation. Thus any correlation measurement between two spatially separated probes will, of necessity, measure some averaged k for any given ω.

It should be noted that all of the correlation and coherence measurements reported in this thesis are of the radial magnetic fluctuations.

4.2.1 Radial correlations and coherence

A probe with four coaxial coils each separated radially by one centimeter in a 1/4" sheath was used to determine the radial correlations of the radial magnetic fluctuations for the frequency range 0.5 to 2.0 MHz in a discharge with q_a=1.1. The coil at the smallest radius was used as the reference coil. Figure 4.9 shows the crosscorrelations for these coils when the reference coil was placed at x=6 cm (inside the separatrix) along the midplane. The radial correlations are small. No attempt was made to determine a radial correlation length for these data due to the lack of any significant correlation for signals inside the separatrix. The coherence for various frequencies is shown in Figure 4.10. Only for the lowest frequencies

was there any significant coherence between adjacent coils. Coherence lengths for the two lowest frequency cases shown are about one centimeter. At frequencies above 780 kHz, the coherence lengths are much smaller. This seems to imply that the higher frequency radial fluctuations have very short radial scale lengths.

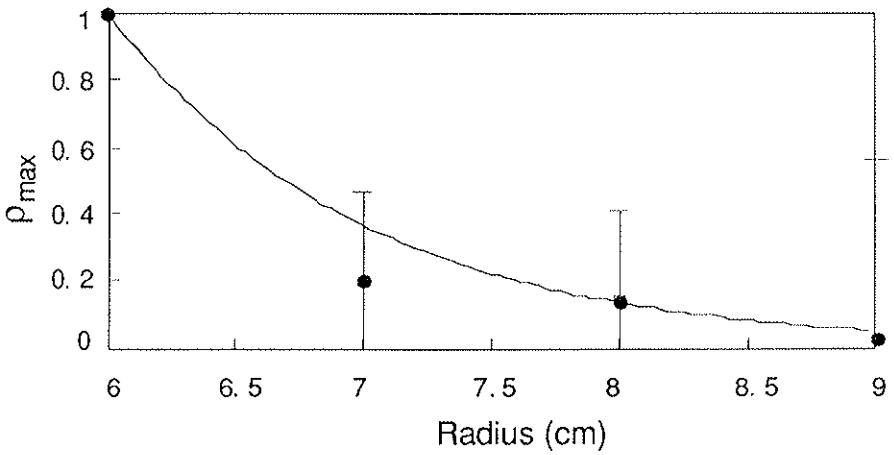

Figure 4.9 Radial correlations for the high frequency fluctuations inside the separatrix of a discharge with q_a=1.1. The curve is for a 1 cm correlation length

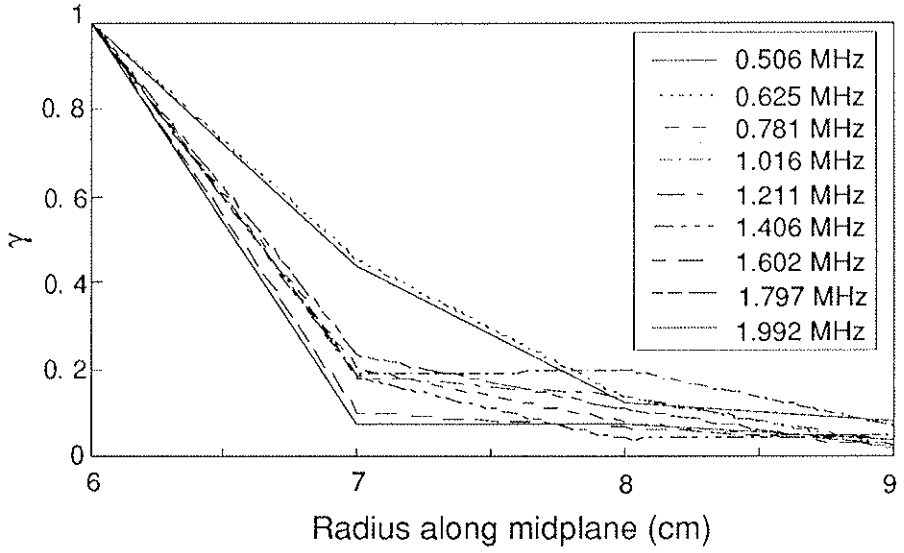

Figure 4.10 The coherence for radially separated probes shows that the coherence lengths for the higher frequencies are very short.

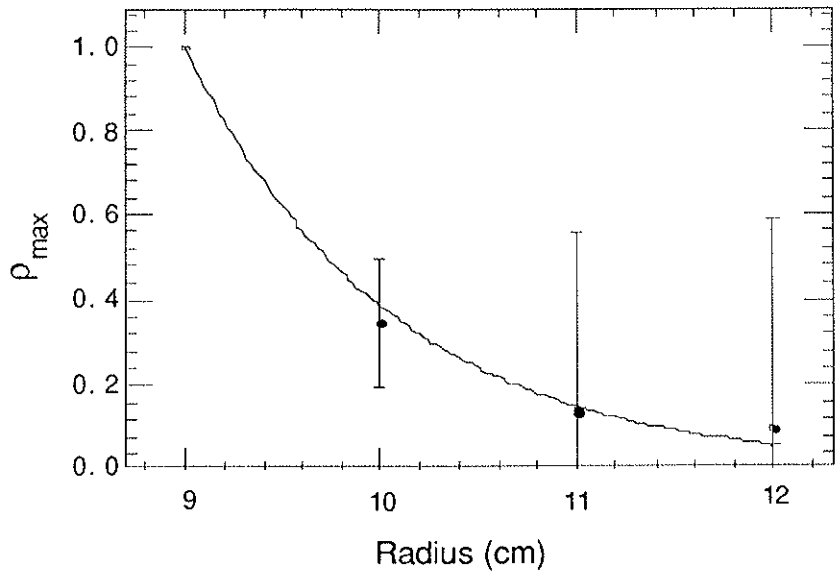

Figure 4.11 Radial correlations for the high frequency fluctuations outside the separatrix of a discharge with q_a=1.1. The curve represents a 1 cm correlation length.

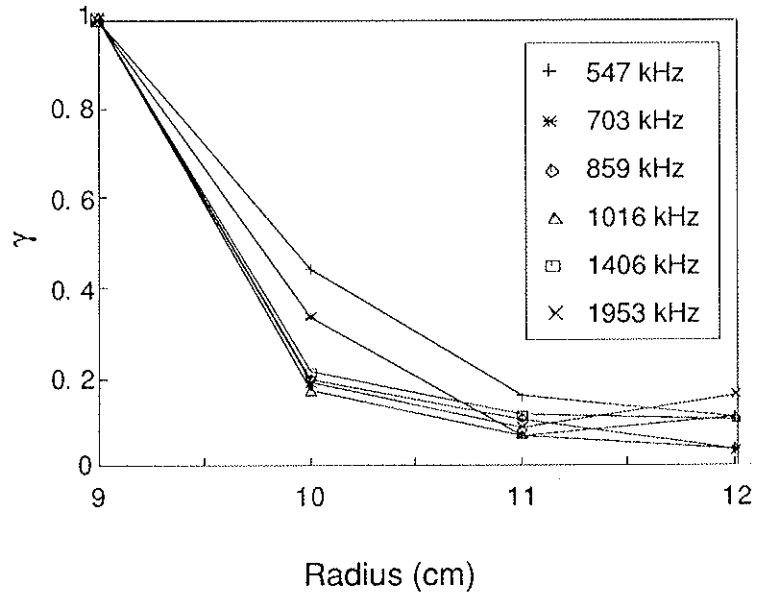

Figure 4.12 Coherence for radially separated probes outside the separatrix

When the probe was moved so that the reference coil was at x=9 cm (the assumed location of the separatrix), the radial correlations could then be made for the edge region in Tokapole II. Figure 4.11 shows that the correlation length outside the separatrix is about one centimeter for this range of frequencies. Figure 4.12, shows that it is only the lowest frequencies which are coherent over distances that could be measured with this probe separation.

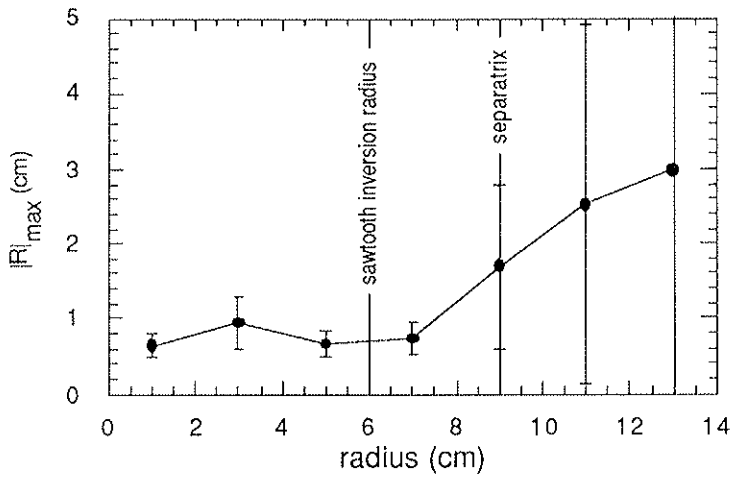

Figure 4.13 Radial correlation length profile in a discharge with q_a=1.3

A boron nitride clad mini probe with radial coils separated by 0.3 mm was used to measure the profile of the radial correlation length for low frequency magnetic fluctuations. The probe was moved from x=12 cm to x=0 cm in two centimeter steps in a discharge with q_a=1.3. (Note: this was the same data set used to determine the effect of the

miniprobe insertion on the global and edge characteristics reported in section 3.3.1). Figure 4.13 shows the radial correlation length as a function of radius for low frequency (10 to 500 kHz) magnetic fluctuations.

The radial correlation length decreases sharply from x=13 to x=7 cm. The correlation length inside x=5 cm is comparatively constant, however this may be more of a perturbation effect than a characteristic of the broadband turbulence. The approximate locations of the separatrix and sawtooth inversion radius are shown in Figure 4.13 for informational purposes.

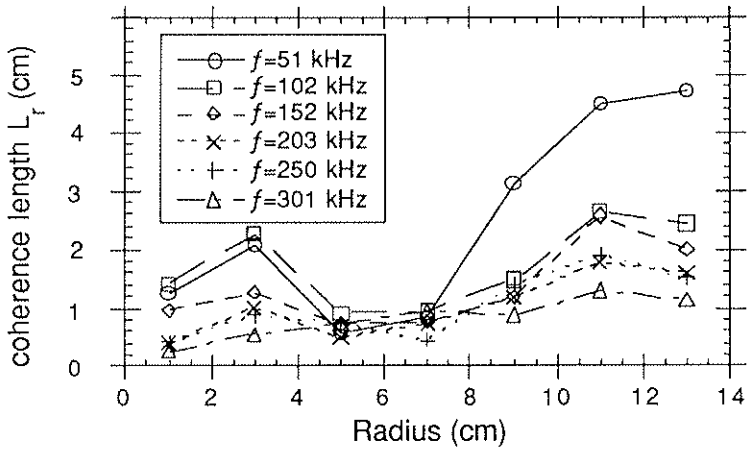

Figure 4.14 The coherence lengths versus radius for selected frequencies demonstrates how the spatial scale changes with both radius and frequency.

Figure 4.14 show the radial coherence lengths at selected frequencies for the same data as Figure 4.13. The coherence length exhibits the same trend as the correlation length in that the coherence

length decreases with decreasing minor radius. This is exhibited at all frequencies up to 2 MHz. The increase in coherence length inside x=5 cm is most likely due to the probe perturbing the plasma.

4.2.2 Parallel correlations and coherence

The measurements of the correlations parallel to the equilibrium field were performed using radial probes placed around the Tokapole II (see Figure 4.15). The initial attempts had a probe at a toroidal angle of 210° from the gap (denoted hereafter as S210) in a fixed position at r=6 cm and swivelled –15° from the midplane with respect the center of the machine (+5° for the probe with respect to the outer wall). Two other probes were located at S240 and T300 (T denotes the top of the machine). These other two probes were swivelled in the r–θ plane. The correlations were then calculated between the fixed probe and the other two probes.

Before presenting the data, it should be noted that once the radial probes are swivelled, they are no longer purely radial and will begin to detect the poloidal field. It then becomes necessary to know what the correlations are between the radial and poloidal components of the magnetic fluctuations. Appendix B shows the complications inherent in the correlation between swivelled probes.

Another complication in measurement of the parallel correlation is the fact that a small change in the pitch angle of the equilibrium field will, over the distances between probes, move the field line past or

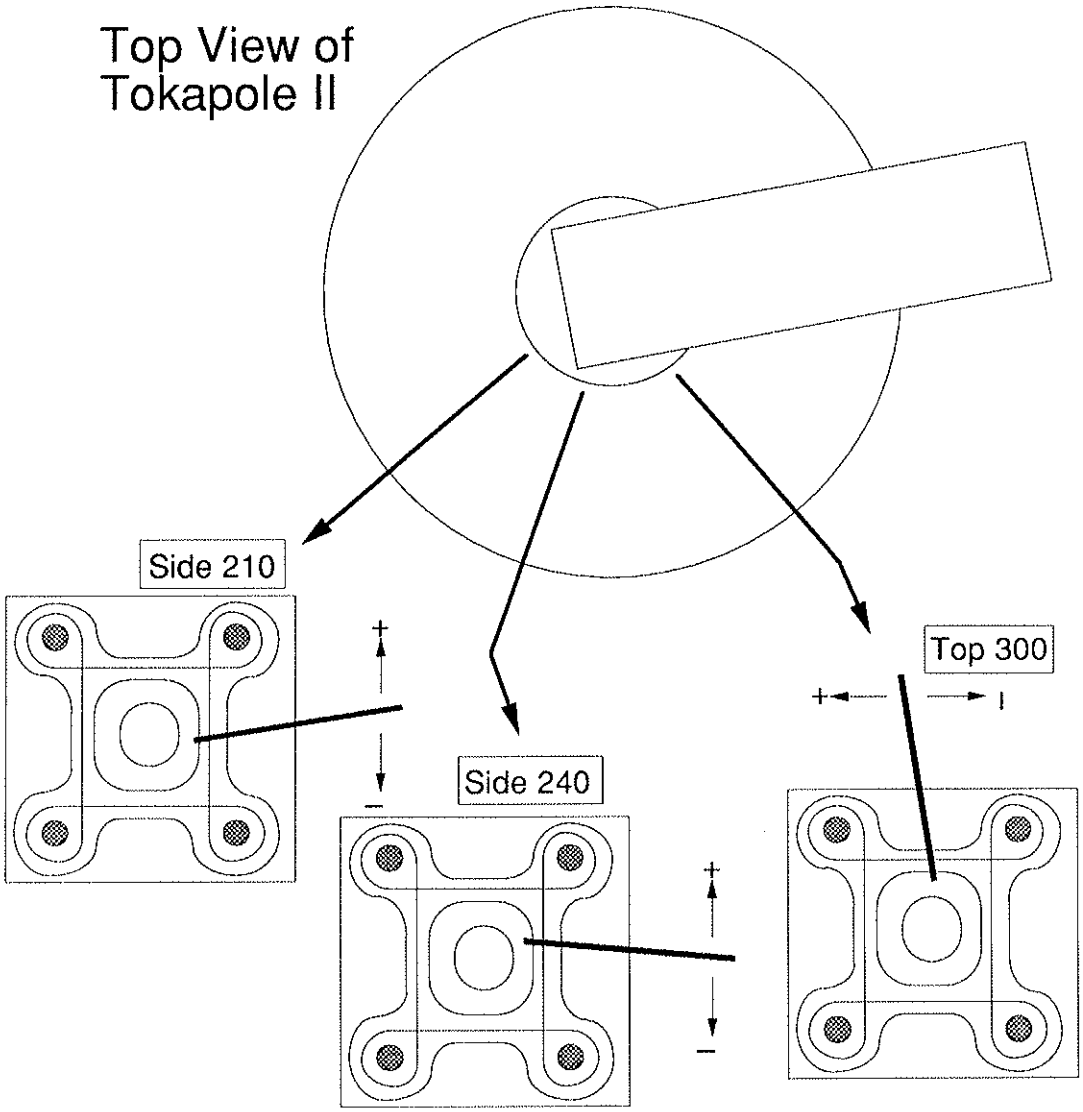

Figure 4.15 Positions of probes to search for the parallel correlation length. This setup was for a q_a=1.1 discharge with the probes positioned along contours of r=6 cm, which is the estimated location of the q=1 surface. The directions of +/− swivel are indicated for each probe with 0° referring to a direction along the midplane (midcylinder) for the probes at the side (top).

away from the probes. To make the attempt possible, reproducible, steady-state parts of the discharges are needed. The problem inherent with the motion of the field lines is illustrated in Figure 4.16.

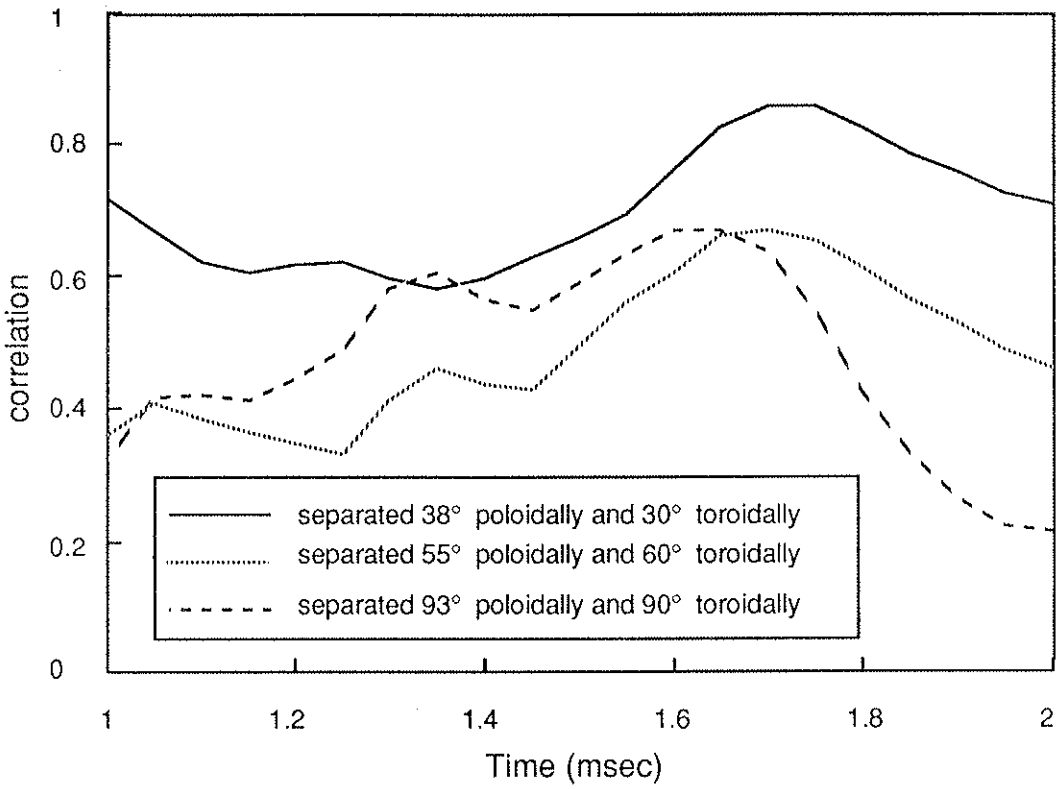

Figure 4.16 The temporal characteristics of the two-point correlation for the three 1/4" probes used to find the peak correlation. This set represents the best case found for three probes. Note that the two cases do not peak simultaneously. The data are from r=6 cm in a $q_a = 1.1$ *discharge.*

Before attempting to measure the correlation parallel to the magnetic field, it is useful to measure the correlations between probes which are known not to be on the same field line. The probe at S240 was swivelled to –15° from the midplane (the same as S210) which gave probes with only a toroidal separation. Due to the pitch of the field line,

these two positions, although on the same approximate surface, are not on the same field line. Figure 4.17 shows the coherence for toroidally separated probes. Only the lowest frequencies show any coherence between the probes. This result will be needed later to show that it is not just a single, or possibly a few, frequencies which give the high correlations.

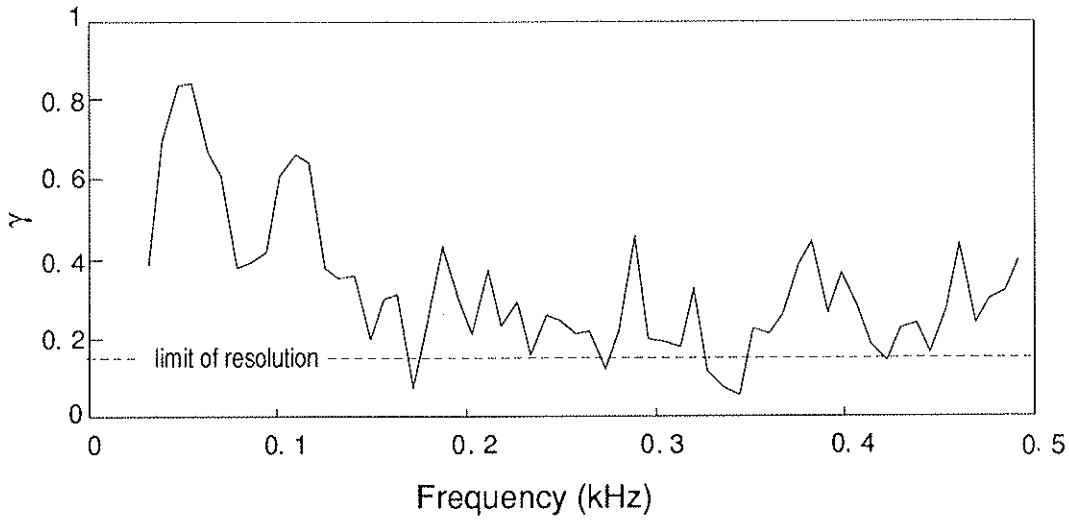

Fgure 4.17 Coherence for two probes separated by 30 degrees toroidally and 0 degrees poloidally

With the probe at S210 fixed, the probes at S240 and T300 were swivelled in the r–θ plane. Figure 4.18 shows the correlation between the probes separated by 30° toroidally. The extent of the correlation is about 20° to 30° poloidally, which for x=6 cm, the radius where the probes are positioned, gives L_p, the poloidal correlation length, about 2 to 3 cm for the radial magnetic fluctuations. This is consistent with

the three to four centimeters measured by Graessle[1] with probes at the same toroidal azimuth which lends credence to the measurement technique.

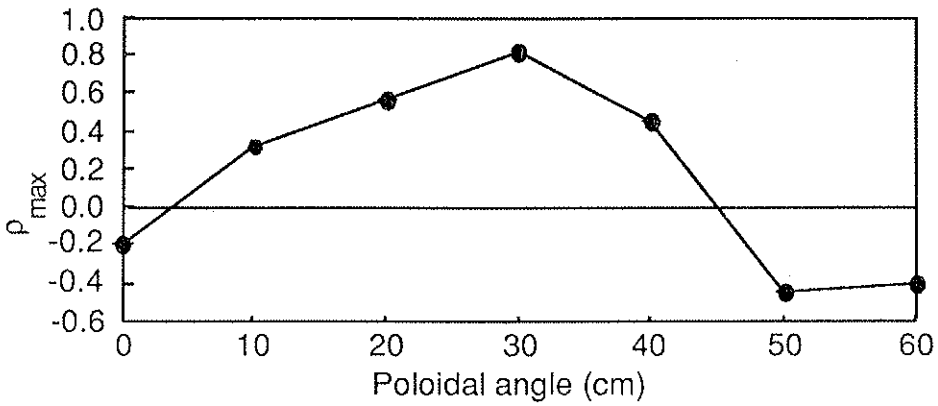

Figure 4.18 With the coils separated by 30° toroidally, the correlation peaks at a poloidal separation near 30°. This implies the direction of maximum correlation is very near the expected q=1 field line.

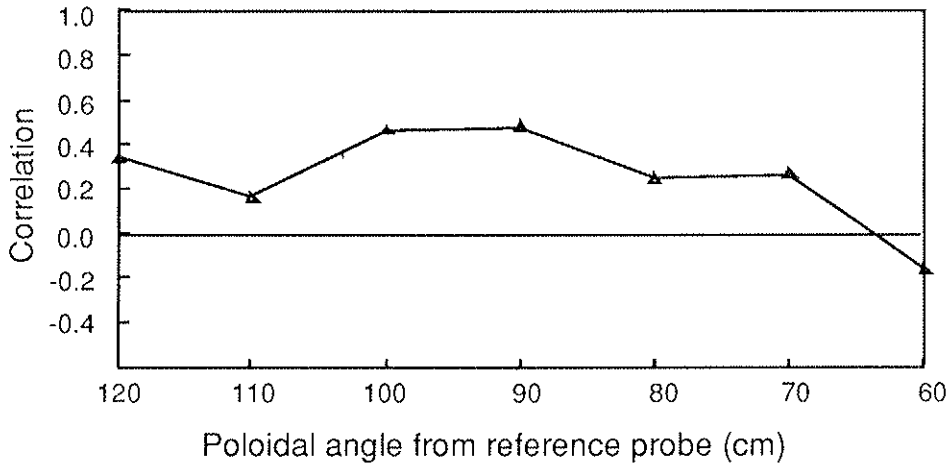

Figure 4.19 With probes separated by 90° toroidally, the peak in the correlation maximum for q=1 is not so clear. It is between 90° and 100° poloidally but has broadened significantly.

For the probes separated by 90° toroidally (Figure 4.19), the structure of the correlation is not as well defined. Although there are many possible reasons for this, the largest is probably due to the deviation of the magnetic field pitch with time.

Taking the largest values of the correlation found for the radial magnetic fluctuations, the parallel correlation length, denoted by L_0, can be calculated. The values are shown in figure 4.20. The line is a fit to points with probe 1 (at S210) as the reference and gives a value of $L_0 = 190 \pm 10$ cm. The direction of this correlation is indistinguishable from the direction of the magnetic field to the degree that the equilibrium field is known in Tokapole II.

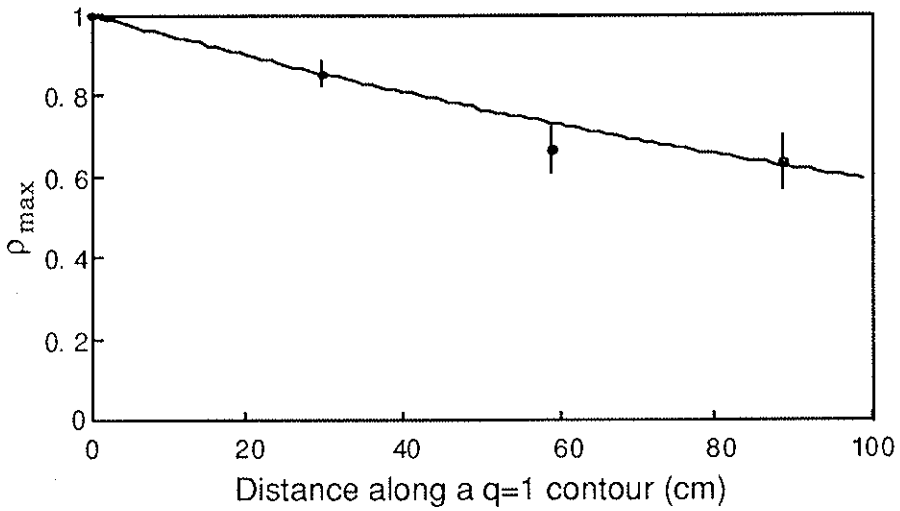

Figure 4.20 Correlation along a q=1 contour shows the extended nature of the parallel correlation length. The data were taken in a q_a=1.1 discharge.

Using the same discharge settings and probe positions, the

correlations were measured for the fluctuations in the frequency interval $0.5 \leq f \leq 2.0$ MHz. It is shown in figure 4.21 that for the higher frequencies L_0 is 30 ± 10 cm. From the radial result presented previously it was shown that the higher frequencies have a smaller spatial scale than those at the lower frequencies. This would make the parallel correlation measurement much more sensitive to probe location and variations of the magnetic field pitch. It may not be possible to measure properly the high frequency parallel correlations by this method.

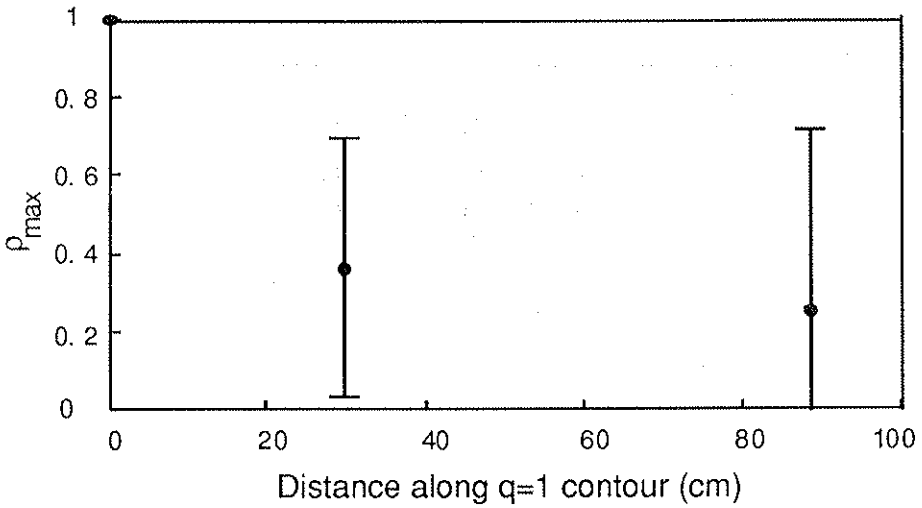

Figure 4.21 Correlation along a q=1 contour for high frequency (0.5–2.0 MHz) fluctuations. The correlation length is about 30 cm for this frequency interval.

To determine if the measured correlations are due to a relatively few modes or are indicative of the broadband fluctuations, the coherence was calculated. For the low frequency fluctuations, the coherence was high, greater than 0.7, for the entire frequency interval

as shown in figure 4.22. Thus the correlations reported above are truly indicative of the broadband fluctuations. The higher frequencies showed a significant coherence (figure 4.23) only for the lower frequencies in the frequency interval 0.5 to 2.0 MHz.

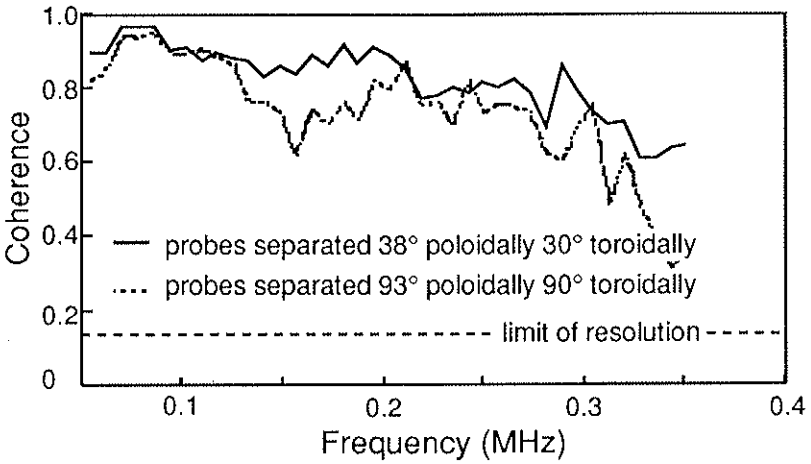

Figure 4.22 The coherence between probes near the q=1 contour show high coherence over the entire frequency interval 50 to 300 kHz.

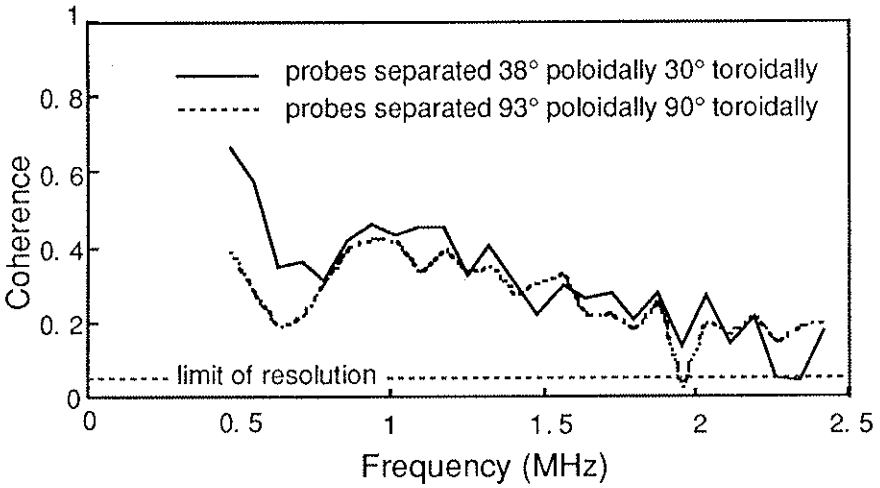

Figure 4.23 Coherence for high frequencies (0.5–2.0MHz) between helically separated probes are significantly lower than for the lower frequencies.

A probe which consisted of three co-linear mini probes (referred to as the forked probe) was used to measure the correlation of the radial magnetic fluctuations with relatively closely spaced coils. For the data presented The forked probe was placed at two positions, x=6 cm and x=8 cm, in a discharge with q_a=3 and an 80:1 turns ratio on the poloidal windings. The forked probe was then rotated so that the correlation with respect to the local pitch angle of the magnetic field could be measured.

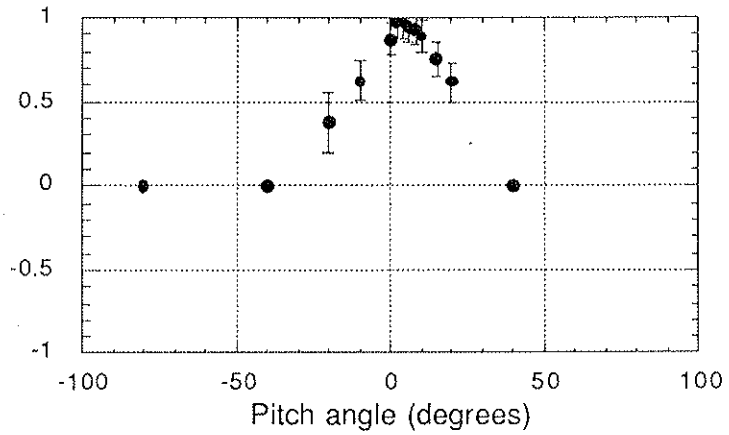

Figure 4.24 The correlation versus local pitch angle at x=6 cm in a q_a=3.0 discharge.

With the forked probe at x=6 cm, the correlation shows a marked peak at an angle of about 3° with respect to the toroidal direction (figure 4.24) and falls off smoothly as the probe is rotated in either direction. Calculating the coherence (figure 4.25) shows that this peak varies by no more than 2° for frequencies between 40 and 300 kHz. One can show, assuming cylindrical symmetry which really is not appropriate for Tokapole II, that the local field pitch is given by $\tan\theta = n/qR$ where q

is the safety factor at the radius of the probe.

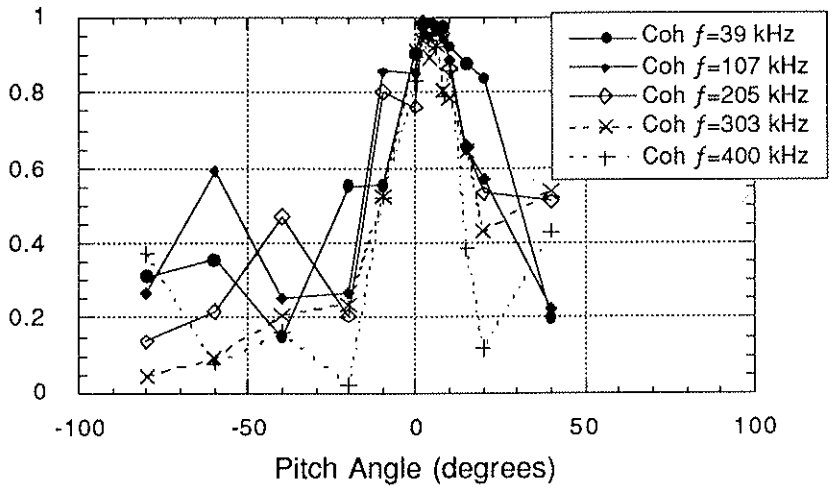

Figure 4.25 The coherence versus local pitch angle shows that the peak in the correlation is present at all frequencies.

J.A. Goetz[2] has measured the q profile for a q_a=3 discharge in Tokapole II and shows $q_{x=6cm} \approx 1.4$. For r=6 cm and R=56 cm the local pitch angle of the field is approximately q = 4.7°. The estimated positioning (human) error is about 2°. So, to the accuracy of the experiment, the direction of the peak in the correlation is indistinguishable from the direction of the equilibrium field. It should be noted that the q_a=3 discharge used to measure the q profile, had a 40:1 primary turns ratio and approximately 60% of the plasma current of the q_a=3, 80:1 discharges used for this data. An assumption is being made here that the two discharges have similar q profiles.

The parallel correlation length given by this result is $L_0 = 60 \pm 20$

cm. This is a surprise because it is widely assumed that L_0 is about qR. However, because of the proximity of the two probes, the correlation is very high, ρ_{xy}=0.966. When the correlation is this high the correlation length is extremely sensitive to the value of the correlation. For example if the correlation had been ρ_{xy}=0.986, a change of only 0.02 and well within the statistical uncertainty of the measurement, the correlation length then becomes 145 ± 116 cm. Thus, although the correlation is very high, an accurate estimate of the correlation length is not possible. No coherence lengths are calculated for these data for similar reasons.

Because the correlation and coherence are so high, the phase measurement and hence the estimation of $k_{||}$ becomes very accurate. The dispersion relation, k(f) for the frequency interval is shown in figure 4.26 where k is calculated from k=θ(f)/Δx and Δx is the probe separation. For these data the frequency averaged $\bar{k}_{||}$ is about 0.05±0.02 cm^{-1}.

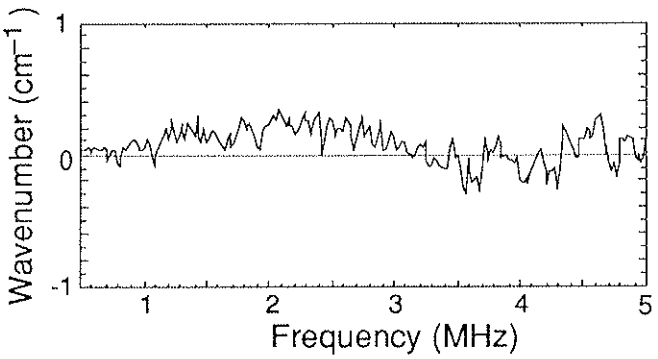

Figure 4.26 Dispersion relation for the high frequency magnetic fluctuations. Data are from the forked probe at x=6 cm in a discharge with q_a=3.0 with the probe oriented nearly parallel to the equilibrium field.

Before the above results were obtained, the forked probe was placed at x=8 cm in similar q_a = 3 discharges. The correlations versus pitch angle of the probe are shown in figure 4.27. There is no indication of a peak; rather the correlation is constant at either of two values, +0.5 or –0.3. The angular width of either the +0.5 or the –0.3 region is approximately 90°. The time lag for the correlation was approximately zero for both the +0.5 and –0.3 correlations and only deviated appreciably from zero near the transition points. The data labelled as being taken at the end of March were for supposedly the same discharges with the probes in the same position as for the other data, but taken a month later. Figure 4.28 shows the coherence for these data. No obvious angular dependence is evident.

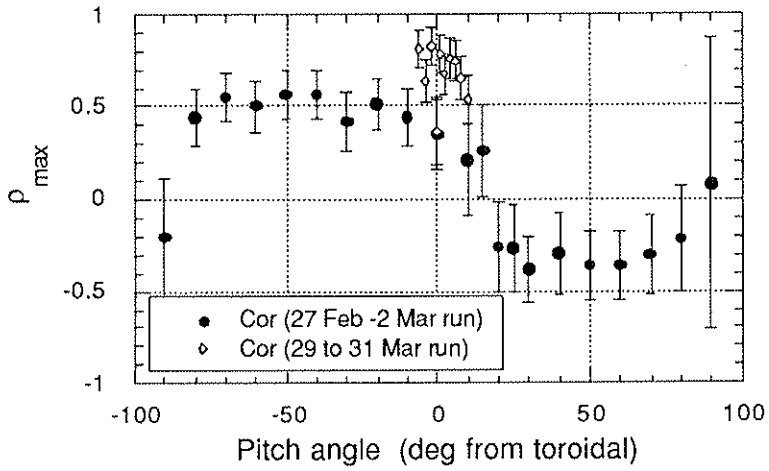

Figure 4.27 Correlation versus pitch angle of the forked probe at x=8 cm in a discharge with q_a=3 shows no discernible peak for the 27 Feb–2 Mar data run. The 29–31 Mar data run showed a higher correlation but was still constant with angle.

From the q profile, $q_{x=8\ cm}$ is about 3. However x=8 cm is also close to the estimated location of the separatrix at x=9 cm. Thus the q value is most likely varying more from shot to shot here than elsewhere in the discharges. This may be the cause for the differing results from the different data. The data either inside (r < 8 cm) or outside (r > 10 cm) the separatrix (x=9 cm) showed better reproducibility from shot to shot and day to day.

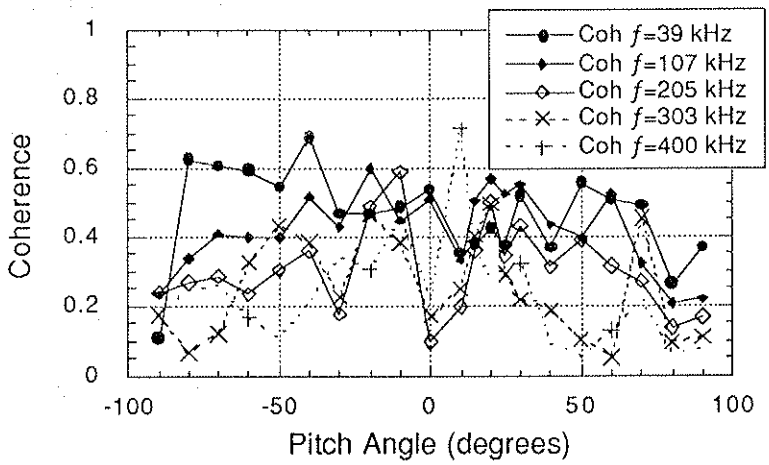

Figure 4.28 The coherence for x=8 cm shows that general features are absent over the entire frequency range measured.

4.3 Discussion of results and transport estimates

4.3.1 General observations on the 0.5 – 5.0 MHz fluctuations

With the exception of one data run, the magnetic fluctuation amplitude in the frequency range 0.5 – 5.0 MHz monotonically

decreased with increasing frequency. The fluctuations above 0.5 MHz are much more sensitive to the edge safety factor than was shown previously for the fluctuation levels below 0.5 MHz. The scaling of the magnetic fluctuations with the plasma current is approximately the same for both frequency ranges which leads one to believe that the plasma current, although possibly a source of free energy, is not the main variable which determines the magnetic fluctuation levels.

The density, over the course of all the discharges presented in this thesis, only changed by at most a factor of five to ten while the high frequency magnetic fluctuations changed almost four orders of magnitude. Thus it is doubtful that, although the fluctuation profiles tend to follow the equilibrium profiles, the equilibrium density has a significant effect on the fluctuations levels. This question of whether the density fluctuations are important in the scaling of the magnetic fluctuations will not be answered in this thesis due to a lack of internal density fluctuation measurements. Other experiments have shown little relation between density and magnetic fluctuations in the edge regions of tokamaks.[3–5] Also, it has been shown elsewhere[6] that the density fluctuations peak where the density gradient is the largest. This is not the case for the magnetic fluctuations which tend to peak in the center of the machine.

The temperature profile and fluctuations, especially in the interior region where the magnetic fluctuations are the largest, are lacking on Tokapole II. Thus no attempt at a scaling with the equilibrium temperature profile or the temperature fluctuations was undertaken.

The extreme sensitivity to the edge safety factor, and not to other plasma quantities, lends itself to the idea that it might be the field topology which determines the magnetic fluctuation level. Profiles of the safety factor for Tokapole II were made by Osborne[7] ($q_a < 1$, pre–1987 upgrade) and Goetz[2] ($q_a = 3$, post upgrade). For the low q_a case it was shown that the safety factor was constant over most of the radius and rose sharply near the separatrix, consistent with the profiles for magnetic fluctuations at low q_a. The case with higher q_a showed a profile which was relatively constant only from about the center out to six centimeters and then rose less sharply than the case with lower q_a. This is consistent with the high frequency magnetic fluctuation profiles measured here and the low frequency fluctuations previously presented by Graessle.[1]

4.3.2 Comparison with thermally excited Alfvén waves

The frequency integrated fluctuation level was calculated by Agim[8] for thermally excited shear Alfvén and fast magnetosonic waves. He found, for the thermally driven magnetic fluctuations and using values consistent with those for Tokapole II, the fluctuation level normalized to the equilibrium field should be on the order of 10^{-10}. The lowest experimental fluctuation level found over the frequency range 0.5 to 5.0 MHz was 10^{-7} for $q_a = 3.8$. The theoretical calculation bounded the available k–spectrum for the Alfvén modes by the relation $\omega\left(\approx kv_A\right) \leq \omega_{ci}$ where v_A is the Alfvén speed and ω_{ci} is the ion cyclotron

frequency. This gives the relation for the wavenumbers as $k \leq \omega_{pi}/c$ where $\omega_{pi} = \left(4\pi n_i e^2/m_i\right)^{1/2}$ is the ion plasma frequency.

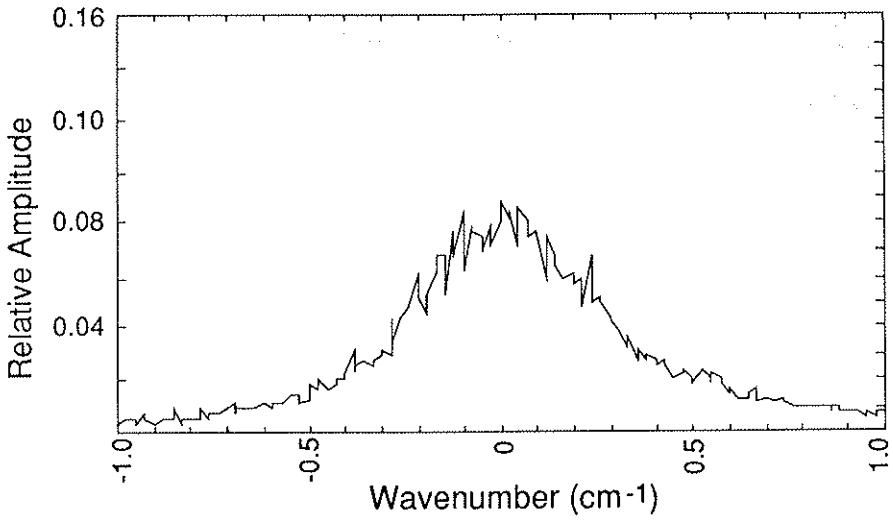

Figure 4.29 Parallel wavenumber spectrum for the magnetic fluctuations (0.5 – 5.0 MHz) shows no preferential direction along the equilibrium field line. The data is from the forked probe at x=6 cm in a discharge with q $_{\bar{a}}$=3.0

For a density of 1×10^{13} cm^{-3}, which is the the largest line averaged density used experimentally, the theoretical $|k_{max}|$ is about 0.14 cm^{-1}. The measured parallel wavenumber spectrum (figure 4.29) for 0.5–5.0 MHz signals shows significant power up to $k \approx 0.5$ cm^{-1}. For discharges with $q_a = 3.8$, where the fluctuation power was the lowest measured, the toroidal field was 5500 gauss and the line averaged density was 2×10^{12} cm^{-3} which gives v_A of 8.5×10^8 $cm\ s^{-1}$ and ω_{ci} of 5.3×10^8 $rad\ s^{-1}$. Then kv_A ($= 4.2 \times 10^8$ $rad\ s^{-1}$) is less than the ion cyclotron frequency so that the bounds imposed by the model

should still be satisfied.

The fact that the measured fluctuation power is still three orders of magnitude larger than for thermally driven estimates in this frequency range implies that there is some other source of free energy driving the broadband fluctuations. Exactly what is driving the broadband fluctuations is still not known, and this question will not be answered in this thesis.

4.3.3 Estimation of thermal diffusion from stochastic fields

Before calculating the thermal diffusivities based on these experiments, it is necessary to determine which turbulence regime is appropriate for these discharges. The mean free path for electrons is given by[9] $\lambda_{ei} \approx 4.5\times10^{13}T^{3/2}/n \ln\Lambda$ (cm) where n is the density in cm^{-3}, $\ln\Lambda$ is the coulomb logarithm and T is the electron temperature in eV. For the discharges used in this thesis the mean free paths were between 10^3 cm (q_a=1.1) and 10^4 cm (q_a=3.0). The ratio between the mean free path and the parallel correlation length determines whether the plasma is considered collisional or not. The longest measured correlation length is $L_0 = 190 \pm 10$ cm for q_a=1.1. Thus for all plasma parameters used in this thesis, λ_{ei} is greater than L_0, and hence only collisionless estimates will be used.

Another consideration is whether the measured fluctuations are in the quasilinear (weak) or the strong turbulence regimes. The distinction is the ratio of the perpendicular scale length to the parallel correlation

length. If this ratio is larger than the magnetic fluctuation amplitude normalized to the equilibrium field, then a quasilinear approach is valid. For the discharges with q_a=1.1, L_0 is 190 cm, δ_{perp} is about 3 cm (from the radial correlation length) and $\tilde{B}/|B|$ is 10^{-3} which is less than δ_{perp}/L_0 (=0.016), so that the fluctuations are in the quasilinear regime.

The thermal diffusivity estimate for the collisionless, quasilinear regime is given by Rechester and Rosenbluth[10] as

$$\chi_c = v_e L_0 \left(\frac{\tilde{B}}{|B|}\right)^2 \qquad (4\text{–}4)$$

For discharges with q_a=1.1 (L_0=190 cm, $v_{th,e}$=3.3×10^8 cm/sec, and $\tilde{B}/|B|$ = 5×10^{-3}), the low frequency (10 to 400 kHz) contribution to the thermal diffusivity is χ_e = 1.6×10^6 cm^2/sec. The global estimate of the diffusivity necessary to explain the confinement, χ_e (= a^2/τ_E), is 1×10^6 cm^2/sec where a is the minor radius and τ_E is the global estimate of the electron energy confinement time. For discharges with q_a=1.1, a stochastic estimate for the confinement is sufficient to describe the measured global energy transport. This result is not new and was previously reported by Graessle.[1]

For discharges with q_a=3.0 ($v_{th,e}$ = 3.9×10^8 cm/sec, $\tilde{B}/|B|$ = 3×10^{-4}), assuming that the true parallel correlation length for q_a = 3.0 is at least as large as that for q_a=1.1, χ_e is then 6.7×10^3 cm^2/sec. The global estimate gives χ_e to be 3×10^5 cm^2/sec. The contribution from the high frequency fluctuations with $\tilde{B}/|B|$ = 10^{-7} adds a negligible amount to the diffusivity. Thus, the quasilinear estimates for the electron energy

transport are unable to explain the global energy transport at all edge safety factors attainable on Tokapole II.

Although it was shown that the magnetic fluctuations are in the quasilinear regime, it is interesting to calculate the thermal diffusivities using the strong turbulence model. For the collisionless strong turbulence limit the thermal diffusivity is defined as[11]

$$\chi_c = v_c \delta_\perp \frac{\tilde{B}}{|B|} \tag{4–5}$$

where $\delta_\perp$ is the perpendicular scale length of the fluctuations. Using the radial correlation length of 3 cm reported in this thesis, the thermal diffusivity for discharges with q_a=1.1 becomes 5×10^6 cm^2/sec. This would easily explain energy transport in Tokapole II for the low q_a cases. Further, for q_a=3.0, the thermal diffusivity becomes 3.5×10^5 cm^2/sec. This is interesting because it compares very favorably with the global estimate of 3×10^5 cm^2/sec. Thus, if one makes the assumption that the energy losses are dominated by the electron thermal conduction, the scaling of the diffusivity necessary to explain the transport should go as $\tilde{B}/|B|$ similar to the strong turbulence result rather than $\left(\tilde{B}/|B|\right)^2$ from the quasilinear result.

References

[1]D.E. Graessle, PhD Thesis, *Magnetic Turbulence Versus Safety Factor in the Tokapole II Tokamak*, University of Wisconsin-Madison, (1989); D.E. Graessle, S.C. Prager, R.N. Dexter, Phys. Rev. Lett., **62**, 535 (1989).

[2]J.A. Goetz, *Total Magnetic Reconnection During a Tokamak Major Disruption*, submitted to Phys. Rev. Lett.

[3]S.J. Zweben, R.J. Taylor, Nucl. Fusion, **21**, 193 (1981).

[4]S.J. Zweben, C.R. Menyuk, R.J. Taylor, Phys. Rev. Lett., **42**, 1270 (1979).

[5]Y.J. Kim, K.W. Gentle, C.P. Ritz, T.L. Rhodes, R.D. Bengtson, Nucl. Fusion, **29**, 99 (1989).

[6]A.J. Wootton, B. Carreras, H. Matsumoto, K. McGuire, R. McKnight, W.A. Peebles, Ch. Ritz, P.W. Terry, and S. Zweben, *Fluctuations and Anomalous Transport in Tokamaks*, Report #340, Fusion Research Center, University of Texas at Austin (1989), submitted to Phys. Fluids.

[7]T.H. Osborne, PhD Thesis, *Disruptive Instabilities in a Poloidal Divertor Tokamak*, University of Wisconsin-Madison (1984).

[8]Z. Agim, PhD Thesis, *Two-Dimensional Magnetohydrodynamic Equilibria with Flow and Studies of Equilibrium Fluctuations*, University of Wisconsin-Madison (1989); Y.Z. Agim, S.C. Prager, Phys. Fluids B, **2**,1138 (1990).

[9]D.L. Book, *NRL Plasma Formulary*, Naval Research Laboratory publication number 0084-4040 (1987).

[10]A.B. Rechester and M.N. Rosenbluth, Phys. Rev. Lett., **40**, 38 (1978).

[11]J.A. Krommes, C. Oberman, R. Kleva, J. Plasma Physics, **30**, 11 (1983).

Chapter 5: Summary and Further Experiments

This chapter presents a summary of the magnetic fluctuation results obtained on the Tokapole II tokamak. The results are for the most part not unexpected. These experiments were motivated mainly by two factors. First, there is a decided lack of magnetic fluctuation measurements from the interior region of tokamaks and other magnetic confinement devices. Second, local probes can be inserted well into the Tokapole II tokamak without adversely affecting the global characteristics of the plasma. The second factor makes the Tokapole II tokamak an ideal machine to help to eliminate, at least in part, the lack of local information in the interior regions of tokamaks. It was this ability which enabled D. Graessle[1] to characterize the magnetic fluctuations in the frequency range from 10 to 500 kHz. Some of the results presented here extend the results found by Graessle up to 2 MHz.

5.1 Review of results

Edge safety factors between 0.8 and 3.8 have been achieved in the Tokapole II. The magnetic fluctuations between 0.5 and 2.0 megahertz, normalized to the equilibrium fields, decrease by over three orders of magnitude as the edge safety was increased by over a factor of 4. The magnetic fluctuation amplitude scales as $q_a^{-4.1}$, which was more sensitive to the edge safety factor than found by Graessle[1] for the lower

frequencies. The amplitude of the fluctuations above 500 kHz was between a factor of 10 (q_a about 0.8) to 1000 (q_a about 3.8) lower than the fluctuation amplitude found by Graessle.[1] Because the magnitudes of the magnetic fluctuations are lower at frequencies above 500 kHz, the contribution of the higher frequency fluctuations to the total estimated stochastic transport[2] is essentially negligible.

The spectra above 500 kHz were featureless (except for one data set) and decreased monotonically with increasing frequency. Although the spectra for a given safety factor varied in amplitude with radius, the shape of the spectra was independent of radius for all cases measured here. The radial profiles showed the radial and poloidal magnetic fluctuations increased with decreasing radius. The profiles of the magnetic fluctuations generally followed the equilibrium density profiles which are assumed to exist at the various edge safety factors in Tokapole II. Detailed internal measurements of the equilibrium density and temperature profiles are lacking for Tokapole II and represent some of the more crucial data that are needed to understand the transport.

The high frequency fluctuation level was compared with the theoretical fluctuation level derived from thermally driven Alfvén and magnetosonic waves.[3] Even for the lowest fluctuation level found experimentally, the theoretical estimate was at least three orders of magnitude smaller than the measured fluctuation levels.

Radial correlation lengths of the high frequency, radial magnetic fluctuations were extremely short. The measured values were less than

or equal to one centimeter for the fluctuations outside the separatrix and strictly less than one centimeter for fluctuations inside the separatrix. By contrast, the radial correlation lengths for low frequencies were shown to be on the order of two to three centimeters outside the separatrix and less than or about one centimeter inside the separatrix. The low frequency results agree with the low frequency results reported by Graessle.[1]

A measurement of the parallel correlation length of the radial magnetic fluctuations was made at a radial location corresponding to r/a = 0.67. The value for the correlation length of the low frequency radial fluctuations in a discharge with edge safety factor of 1.1 was found to be 190±10 cm. The correlation length for the radial magnetic fluctuations above 500 kHz was much shorter with a value of about 30±1 cm. The coherence for probes displaced along a field line was high for all frequencies in the interval 10 to 400 kHz. For fluctuations in the interval 0.5 to 2.0 MHz the coherence was significantly lower and tended to decrease with increasing frequency. The direction of the maximum correlation was indistinguishable from the direction of the local field line. The parallel wavenumber for discharges with q_a=3.0 was shown to be small, about 0.05 ± 0.02 cm^{-1}

5.2 Conclusions

From the results presented in this paper there are several general conclusions which can be made:

(1)While it is undetermined whether the magnetic fluctuations contribute to the overall energy loss from a tokamak plasma, it is clear that the magnetic fluctuation levels are dependent on whatever the causes of the energy losses are.

(2) The fluctuations from 0.5 to 5.0 MHz are being driven by something other than the thermal spectrum derived for Alfvén and magnetosonic waves.

(3) The profiles of the various components of the magnetic fluctuations seem to indicate that the magnetic fluctuations may be stabilized by the magnetic shear.

(4) The scale lengths of the magnetic fluctuations decrease with increasing frequency.

(5) The parallel correlation length of 190 ± 10 cm should be considered a lower bound. Discharges which were more reproducible may result in a better measurement because of the reduced field line flutter.

(6) The forked probe results seem to indicate that the field lines are reasonably well defined inside the separatrix, while near the separatrix the field lines may be stochastic.

5.3 Suggestions for future work

As with most experiments, the results presented here bring about more questions than are answered. It is still unknown what is driving the broadband magnetic fluctuations. It is not known whether the broadband magnetic fluctuations are a cause or effect of the transport

mechanisms. To this end, several future experiments are suggested by some of the results of this work.

First and foremost, the equilibrium density, temperature and current profiles need to be measured over a range of edge safety factors for the entire radius of the Tokapole II. Only then can the various theories on transport be applied with any confidence.

The fluctuation profiles of the density, temperature and plasma current need to be measured over the entire radius of the machine. From the first two, the electrostatic contributions to the transport can be calculated. It is still undetermined whether the electrostatic transport is important in the transfer of particles or energy from the center to the edge of tokamaks. These measurements are currently being attempted by I.H. Tan.[4] A knowledge of the plasma current fluctuations should give detailed information about where the magnetic fluctuations are being generated.

The magnetic shear profiles need to be calculated. The shear is sensitive to the edge safety factor, especially when it has been shown that the central q value does not vary greatly during the quiescent parts of the discharge, regardless of the edge safety factor for Tokapole II.[3,4] Since Tokapole II is a poloidal divertor tokamak, the separatrix is, by strict definition, a $q=\infty$ surface. What the effective edge safety factor is measuring, in a way, is the shear profile. For low edge safety factors, q is very constant with radius and rises sharply near the separatrix. The fluctuations in this case rise to near their maximum values close to the separatrix. For high edge safety factors, the q profile is decreasing with

radius slowly which increases the magnetic shear inside the separatrix. Not surprisingly the fluctuation levels are low at distances well inside the separatrix.

Finally, the bursts which appear on the magnetic fluctuation signals need to be analyzed using a transient analysis similar to that found in Bendat and Piersoll.[5] The bursts are probably due to the excitation of many different modes in the plasma due to the rapid redistribution of the thermal energy across the magnetic island generating the sawtooth activity. If the analysis can be done, a wealth of information on energy transfer and dissipation may become available.

References

[1]D.E. Graessle, PhD Thesis, *Magnetic Turbulence Versus Safety Factor in the Tokapole II Tokamak*, University of Wisconsin-Madison (1989); D.E. Graessle, S.C. Prager, R.N. Dexter, Phys. Rev. Lett., **62**, 535 (1989)

[2]A.B. Rechester, M.N. Rosenbluth, Phys. Rev. Lett., **40**, 38 (1978)

[3]Z. Agim, PhD Thesis, *Two Dimensional Magnetohydrodynamic Equilibria with Flow and Studies of Equilibrium Fluctuations*, University of Wisconsin–Madison (1989); Z. Agim, S.C. Prager, Phys Fluids B, **2**, 1138 (1990)

[4]T.H. Osborne, *Disruptive Instabilities in a Poloidal Divertor Tokamak*, University of Wisconsin–Madison (1984)

[5]J.A. Goetz, *Total Magnetic Reconnection During a Tokamak Major Disruption*, submitted to Phys. Rev. Lett.

[6]Julius S. Bendat and Allen G. Piersoll, *Random Data Analysis and Measurement Procedures, 2nd Edition*, (Wiley–Interscience, John Wiley & Sons, New York, 1986)

Appendix A: Analytical Techniques

The statistical techniques used in this thesis have come from several sources.[1–5] The specific techniques used in the analysis were the power spectra, correlation function, coherence function, and the relative phase. All of these techniques relied on the use of the FFT algorithm for both relative speed of the calculation and to derive the frequency dependence of the measured quantities.

The FFT algorithm in IDL is symmetric with respect to forward and backward transforms. This means that there is a $N^{-1/2}$ scale factor whenever the FFT was used where N is the number of discrete data points in the time record. The equations below are asymmetric with respect to this scale factor. Although there will be no explicit reference to this scale factor elsewhere in this section, it was taken into account in the actual programming so that the equations below are accurate.

6.1 Mean Amplitude and Power Spectra

The amplitude of the fluctuations is given by the equation

$$\tilde{b} = \left\{ \frac{1}{T} \int_0^T b^2(t')\,dt' \right\}^{1/2} \tag{6.1.1}$$

where $\tilde{b}$ is the root-mean-square (RMS) amplitude and $b(t)$ is the

fluctuating magnetic field.

There is no need to resort to spectral analysis for the above calculation as it stands. However, the quantity usually measured is $\dot{b}(t) = db(t)/dt$ so that some form of integration must be used. The method used in this thesis was to calibrate the probe-amplifier-filter system over the frequency ranges of interest, use Fourier analysis to determine the power spectra, and then calculate the total power. If $\dot{B}(f)$ is the Fourier transform of $\dot{b}(t)$ and the complex frequency calibration (amplitude and phase) is represented by $C(f)$ then the amplitude spectrum is given by

$$\tilde{B}(f) = \left\{ \frac{1}{T} (C(f))^2 \left\langle \left| \dot{B}(f) \right|^2 \right\rangle \right\}^{1/2} \tag{6.1.2}$$

where $\langle \ldots \rangle$ represents an ensemble average over many data records. The discrete form of this equation used in the computer calculations is

$$\tilde{B}_n = \left\{ C_n^2 \left\langle \left| \dot{B}_n \right|^2 \right\rangle \right\}^{1/2} \tag{6.1.3}$$

Then the calculation of the fluctuating amplitude is simply given, in discrete form, by

$$\tilde{b} = \left\{ \sum_{n=1}^{N} \tilde{B}_n^2 \right\}^{1/2} \tag{6.1.4}$$

To get the amplitude over a specific range of frequencies is just a matter of adjusting the limits of the summation. The power spectrum is

obtained by squaring the amplitude spectrum, and the power spectral density is obtained by taking the power spectra and multiplying by T,the temporal record length.

6.2 Correlation, Coherence and Phase

To determine possible causal relations between two signals, a more powerful analytical technique is needed. Correlation techniques have proven to be an extremely powerful tool in many areas of spectral analysis. The first of these techniques is the cross–correlation coefficient between two time records which is defined as

$$\rho_{xy}(\tau) = \frac{\left\langle \int x(t)y(t+\tau)dt \right\rangle}{\left\langle \int x(t)x(t)dt \right\rangle^{1/2} \left\langle \int y(t)y(t)dt \right\rangle^{1/2}} \qquad (6.2.1)$$

The denominators are just the amplitudes of each of the signals x and y. This normalization yields values for the correlation of $-1 \le \rho_{xy}(\tau) \le 1$. Note also that the denominators could be written as the $\tau = 0$ un–normalized autocorrelation of the two input functions. The discrete form used is

$$\rho_{xy}(n) = \frac{\left\langle invFFT\left\langle \sum_{i=0}^{N-1} X_i Y_{i+n}^{*} \right\rangle \right\rangle}{\left\langle \sum_{i=0}^{N-1} X_i X_i^{*} \right\rangle^{1/2} \left\langle \sum_{i=0}^{N-1} Y_i Y_i^{*} \right\rangle^{1/2}} \qquad (6.2.2)$$

The coherence function, which is directly related to the correlation function, shows for which frequencies there might exist a causal relation. The coherence function is derived from the complex cross–power spectrum which is given by

$$\Gamma_{xy}(f) = \frac{1}{T}\left\langle X(f) Y^{*}(f) \right\rangle \qquad (6.2.3)$$

from which the coherence function is defined here as

$$\gamma_{xy}(f) = \frac{\left|\Gamma_{xy}(f)\right|}{\left|\Gamma_{xx}(f)\Gamma_{yy}(f)\right|^{1/2}} \qquad (6.2.4)$$

Thus, rather than determine the overall causal relation using the correlation function, the relation over single frequencies or ranges of frequencies can be found. In general the coherency, γ_{xy}^2, is a measure of the percentage of the two input signals which may be causally related. The quantity $\left[1 - \gamma_{xy}^2\right]$ gives the portion of the signals which are not related either due to different sources or from random noise. The relative phase of the two signals at a given frequency is given by

$$\theta(f) = \arctan\left(\frac{\mathrm{Im}\langle \Gamma_{xy} \rangle}{\mathrm{Re}\langle \Gamma_{xy} \rangle}\right) \qquad (6.2.5)$$

The relative phase for random noise should be zero if there are sufficient terms in the ensemble.

6.3 Errors in the statistical quantities

The error estimates of the above quantities are more complicated than just calculating a standard deviation for the mean. Detailed derivations of the error estimates can be found in Bendat and Piersol's text[1] and will not be presented here. First, the error estimate for the coherency is given by[6]

$$\varepsilon\left[\gamma_{xy}^2\right] \approx \frac{\sqrt{2}\left(1-\gamma_{xy}^2\right)}{|\gamma_{xy}|\sqrt{N}} \qquad (6.3.1)$$

Thus the error in the coherency is proportional to the coherency itself. This is understandable since, if the signals are well out of any noise in the system, only a few ensembles would be necessary to determine if a relation between the signals exists. However if the noise level is large compared to the signals, it will take many ensembles for the coherent part of the ensembles to appear out of the noise. The coherence of pure random noise decreases with the number of ensembles as $N^{-1/2}$.

The relative error in the phase measurement is similar to that of the

coherency. The standard deviation in the phase is given by[7]

$$s.d.\left[\theta_{xy}\right] \approx \frac{\left(1-\gamma_{xy}^2\right)^{1/2}}{|\gamma_{xy}|\sqrt{2N}} \qquad (6.3.2)$$

Thus the error in the phase estimate is also dependent on the level of the coherency between the two signals.

The estimate of the statistical error for the correlation is much more complicated. Again without going into a derivation, the general variance estimate for the correlation is

$$var\left[R_{xy}(\tau)\right] \approx \frac{1}{T}\int_{-\infty}^{\infty} \left\{R_{xx}(\xi)R_{yy}(\xi) + R_{xy}(\xi+\tau)R_{yx}(\xi-\tau)\right\} d\xi \qquad (6.3.3)$$

where

$$R_{xy}(\tau) = \frac{1}{T}\int_0^T x(t)y(t+\tau)dt \qquad (6.3.4)$$

is the correlation integral. Equation. 6.3.3 is a little too general and bulky to try to calculate. Instead Bendat and Piersol show that for two sampled signals, $x(t)$ and $y(t)$, of length T which are bandwidth limited with a bandwidth B, the estimate of the error in the cross–correlation is given approximately by[8]

$$\varepsilon[\rho_{xy}(\tau)] = \frac{1}{\sqrt{BT}}\left[1+\rho_{xy}^{-2}(\tau)\right]^{1/2} \qquad (6.3.5)$$

As with the coherence, the relative error is proportional to the value of the correlation coefficient. Note that the error estimate does not depend explicitly on the number of terms used in the ensemble.

6.4 Information derived from the statistical quantities

From the above quantities the scale lengths and, if the coherence is high enough, wavenumbers and phase speeds can be determined for the fluctuations. The scale lengths are determined by fitting an exponential decay to the correlation or coherence assuming one knows the separation of the probes. As an example the correlation length is given by

$$L_d = -x/\ln(|R(\tau_{ext})|) \qquad (6.4.1)$$

where τ_{ext} is the delay time of the extremum of the correlation function, x is the probe separation (note that for probes in a plasma this may not be the direct distance but rather the distance along a magnetic field line) and d represents some appropriate direction of the probes, usually radial, poloidal, toroidal or parallel. The importance of the correlation length, as well as all of the derived quantities, can be found in chapter 2. The coherence length is a frequency dependent quantity and is

calculated similarly to the correlation length.

$$L_d(f) = -x/\ln(|\gamma_{xy}(f)|) \tag{6.4.2}$$

The wavenumber spectrum can be calculated from the relative phase between two signals. If the wavelength is longer than the probe separation x, then the relation $\theta = kx$ is valid. For each frequency for which the coherence is high enough, the relation then becomes

$$\overline{k_d}(f) = \theta(f)/x \tag{6.4.3}$$

where again d denotes some direction. It should be noted that for microturbulence, $k(f)$ does not always have a one–to–one correspondence with frequency. Rather the above equation will determine some average k value for that particular frequency.

From the wavenumber spectra, the mode numbers for a particular direction can be determined. For the poloidal direction, the mode numbers "m" can be determined from the relation

$$m(f) = r\,\overline{k_p}(f) \tag{6.4.4}$$

where r is the minor radius of the probes. Also from the wavenumber spectra, the phase speed of the coherent signals between the two probes can be determined by

$$V_{ph}(f) = \frac{\omega}{\overline{k_d}(f)} \qquad (6.4.5)$$

From the above derived quantities many of the characterizations and estimates of the turbulence can be made. Details are left for chapters 2 and 4.

References

[1]Julius S. Bendat and Allen G. Piersol, *Random Data Analysis and Measurement Procedures, 2nd Edition*, (Wiley–Interscience, John Wiley & Sons, New York, 1986)

[2]E. Oran Brigham, *The Fast Fourier Transform*, (Prentice–Hall, 1974)

[3]E. J. Powers, *Spectral Techniques for Experimental Investigation of Plasma Diffusion Due to Polychromatic Fluctuations*, Nucl. Fusion **14** (1974) 749

[4]William H. Press, Brian P. Flannery, Saul A. Teukolsky, William T. Vetterling, *Numerical Recipes, The Art of Scientific Computing*, (Cambridge University Press,Cambridge, 1986)

[5]Philip R. Bevington, *Data Reduction and Error Analysis for the Physical Sciences*, (McGraw–Hill, New York, 1969)

[6]Bendat and Piersol, p. 310

[7]Bendat and Piersol, p. 301

[8]Bendat and Piersol, p. 273

Appendix B: Correlations of "Mixed" Signals

This appendix concerns the added complication in the correlation analysis when a given probe is measuring two, not necessarily correlated, components of a signal. In particular, when a supposedly radial magnetic coil is swivelled and then starts picking up components of the poloidal field. For two such probes, which are swivelled away from radial by amounts θ and α respectively, the probe signals can be written as

$$\begin{aligned} X_1 &= A_1 B_{r1} \cos\theta + A_1 B_{p1} \sin\theta \\ X_2 &= A_2 B_{r2} \cos\alpha + A_2 B_{p2} \sin\alpha \end{aligned} \tag{B-1}$$

Then using the definition of the correlation from appendix A and performing some algebra gives the result

$$R(X_1,X_2;\tau) = \frac{acR(A,C;\tau)+bdR(B,D;\tau)+adR(A,D;\tau)+bcR(B,C;\tau)}{\left[a^2+b^2+2abR(A,B;0)\right]^{1/2}\left[a^2+b^2+2abR(A,B;0)\right]^{1/2}} \tag{B-2}$$

where

$$\begin{aligned} A = B_{r1} &: a = cos\left(\theta\right)\langle A\rangle \\ B = B_{p1} &: b = cos\left(\theta\right)\langle B\rangle \\ C = B_{r2} &: c = cos\left(\alpha\right)\langle C\rangle \\ D = B_{p2} &: d = cos\left(\alpha\right)\langle D\rangle \end{aligned} \tag{B-3}$$

and

$$\langle \ldots \rangle = \left[\int (\ldots)^2 dt \right]^{1/2} \qquad (B-4)$$

Equation (B–2) is unfortunate in that not only are the correlations between the various field components at both probe locations involved, but the correlation now has an implicit power dependence. If one of the components has significantly more power than the other components, then any correlations of which it is a part will dominate the net correlation.

For the analysis of the swivelled probe data, it was assumed that the power in the radial and poloidal fluctuations was equal. This is true to within a factor of two over all discharge parameters used to obtain the data for this thesis. Measurements of the correlation between the radial and poloidal fluctuations at the same location have been made and shown that $R(B_r, B_p; 0) \leq 0.5$. Correlations between the radial fluctuations of one probe with the poloidal fluctuations of another are significantly lower, and it will be assumed that they are uncorrelated.

These measurements and assumptions, when put into equation (B – 2) gives

$$R(X_1, X_2; \tau) = \frac{\cos\theta \cos\alpha R(B_{r1}, B_{r2}; \tau) + \sin\theta \sin\alpha R(B_{p1}, B_{p2}; \tau)}{\left[1 + \cos\theta \sin\theta\right]^{1/2} \left[1 + \cos\alpha \sin\alpha\right]^{1/2}} \qquad (B-5)$$

The largest correlations were found with all probes angled 15° with

respect to the center of the machine. This then gives the estimate

$$R(X_1, X_2; \tau) = 0.7R(B_{r1}, B_{r2}; \tau) + 0.1R(B_{p1}, B_{p2}; \tau) \qquad \text{(B–6)}$$

It should be noted that even if the correlations of the pure signals are one, the correlation of the mixed signals may still be less than one if the cross correlations between the radial and poloidal components are less than one as was assumed for equation (B–6). The largest correlation measured between two swivelled probes was about 0.86 which would indicate that the cross–correlations of the radial and poloidal components will make a minimum difference of about five percent.

Since the largest dependence is on the radial–radial component, and since the radial–poloidal correlations for displaced probes should be lower than for the radial–poloidal correlations at the same location, the maximum possible error resulting from neglecting the radial–poloidal cross–correlations is 0.1 for each pair or a total of 0.2. From measurements of the radial–poloidal cross–correlations, the estimate of the relative contribution caused by these unwanted correlations is about six percent. This is a systematic error only so long as the cross–correlations are approximately constant with various machine parameters.

The net effect of all of this is to lower the estimate of the true correlation between the radial magnetic fields between two spatially displaced probes. Because the estimated error of six percent is smaller

than the statistical error estimates of ten to twenty percent found for almost all cases presented in this paper, no correction was applied, and all results from swivelled probes shoud be considered a lower bound on the correlation.